UNIVERSITY OF OKLAHOMA

GRADUATE COLLEGE

DURABILITY ASSESSMENT OF 3D PRINTED CEMENTITIOUS ELEMENTS WITH INTERLAYER REINFORCEMENT

A THESIS

SUBMITTED TO THE GRADUATE FACULTY

in partial fulfillment of the requirements for the

Degree of

MASTER OF SCIENCE

By SIJAN ADHIKARI

Norman, Oklahoma

2025

DURABILITY ASSESSMENT OF 3D PRINTED CEMENTITIOUS ELEMENTS

WITH INTERLAYER REINFORCEMENT

A THESIS APPROVED FOR THE
SCHOOL OF CIVIL ENGINEERING AND ENVIRONMENTAL SCIENCE

BY THE COMMITTEE CONSISTING OF

Dr. Shreya Vemuganti, Chair

Dr. Royce W. Floyd

Dr. Aikaterini P. Kyprioti

Acknowledgements

I want to thank my advisor, Dr. Shreya Vemuganti, for her guidance, help, support, and motivation throughout this journey. This work could not have been completed without her guidance and advice, and I am honored to work under her supervision. Also, I would like to thank my committee members, Dr. Aikaterini P. Kyprioti and Dr. Royce W. Floyd, for their support and guidance.

I would like to thank Mr. John Bullock for his assistance in conducting experiments throughout the program. I would like to thank my research team, Benjamin K. Abu, Ali Akbarpour, Trent M. Rogers, and Mumtaheena Reza, for their help and assistance in casting and experimental testing. Lastly, I want to acknowledge and thank Mujtaba Ahmadi, Omar Yadak, and Courtney E. Dawson for assisting and training me. Also, I want to thank my family and friends from home for their unwavering support and motivation.

Abstract

Due to the lack of formwork and the weak morphology at the interface between layers in layer-on-layer extrusion techniques, tensile reinforcement incorporated at the interface between successive layers may be at an increased risk of exposure to environmental conditions like chloride ingress, which affect the durability of such elements, which can be seen in day-to-day conditions. The study addresses two questions: What is the effect of deterioration mechanisms, such as chloride ingress, on the mechanical performance and flexural strength capacities of cementitious binders with successive layers with steel, glass, and carbon fiber reinforced polymer reinforcement incorporated at the interface between successive layers? What are the solutions to mitigate these effects? The methodology of this study involves the development of a thixotropic mix design with rheological and set time parameters suitable for extrusion-based techniques using concrete 3D printing. Subsequently, mechanical and material characterization is conducted on the element after exposure to the deterioration mechanism, i.e., chloride ingress under short-term and long-term exposures. Microstructural analysis at failure interfaces is focused on understanding reinforcement behavior, the bond between binder and reinforcement, and failure modes with exposed vs non-exposed interlayers. In addition, this study reports the suitability of polymer surface finishings and the mismatch of the outer protection system to create an impenetrable barrier system against aggressive ions.

Table of Contents

List of Figures

List of Tables

Preface

During this M.S. (January 2024 – December 2025),

(1) The following reports have been submitted

- January, April, July, and October of 2024 and January, February, April, July, and October of 2025 full and quarterly reports to Southern Plain Transportation Center (SPTC) submitted

(2) The following conference posters and presentations have been delivered

- Poster presentation on Transportation Industry and Workforce Development Symposium - April 30, 2024, University of Oklahoma, Norman, OK
- Poster presentation at the 2024 Summer Transportation Symposium – July 30, 2024, OSU Hamm Institute, Oklahoma City, OK
- Poster presentation on Graduate Student Poster Fair & Networking Event, Sept. 26, 2024, University of Oklahoma, Norman, OK
- Poster presentation on Oklahoma Transportation Research Day (OTRD), Oct. 15, 2024, Grand Ballroom, University of Central Oklahoma, Edmond, OK
- Presentation on ACI Concrete Convention, Fall 2024 for ACI-440D Committee, Marriott Downtown, Philadelphia, PA
- Poster presentation on Advanced Materials, Nov. 15, 2024, West Atrium, Sarkeys' Energy Center, University of Oklahoma, Norman, OK
- Podium presentation on 2025 Summer Transportation Symposium – July 29, 2025, OSU Hamm Institute, Oklahoma City, OK

- 3D printed specimens' demonstration on Oklahoma Transportation Research Day (OTRD), Oct. 14, 2025, University of Central Oklahoma, Edmond, OK

(3) The following conference papers are submitted:

- Adhikari, S., M. Rogers, T., and Vemuganti, S., Durability Assessment of 3D Printed Cementitious Elements with Interlayer Reinforcement, ICTD 2025, T&DI Transportation Conference, Detroit, MI (accepted)

(4) The following journal papers have been published:

- Adhikari, S. et al., Thermoplastic carbon fiber reinforced polymer tapes in cementitious and polymer concretes. Functional Composites and Structures, 2025. **7**(2): p. 025005.[1]
- Adhikari, S., Myers, B. M., Tuck, B. L., Dawson, C., Cipriano, J. R., Ahlert, J. F., ... & Vemuganti, S. (2025). Scanning electron microscopy of carbon nanotube–epoxy interfaces: Correlating morphology to sulfate exposure. *Journal of Composites Science*, *9*(8), 392.[2]

1 Introduction

Bridges, tunnels, culverts, and different structural components form the basic backbone of any country's infrastructure. To ensure public safety and efficient transportation across the United States, the U.S. Department of Transportation (USDOT) emphasizes the importance of designing, constructing, retaining, keeping, and repairing these systems [3]. Because of its strength and flexibility, reinforced concrete has turned out to be a benchmark material in numerous applications. With the development of high-end technologies, techniques that include 3-D printing are emerging as a game-changer to boost the production of reinforced concrete components [4].

3-D printing, also known as additive manufacturing, has gained tremendous interest due to its ability to simplify processes, reduce material wastage, and swift working that traditional methods simply cannot achieve. Similarly, in the context of transportation, 3-D printing offers opportunities for quicker construction, cost efficiency, and improved sustainability. 3-D printing has a variety of branches, which could be the Fused Filament Fabrication (FFF), Selective Laser Sintering (SLS), Concrete 3-D printing, etc., but compared to its counterparts, the real-world applications of 3-D printing in reinforced concrete are still in its early stages, typically considering the long-term durability aspects [4, 5]. 3-D printing offers excellent advantages over conventional construction processes, creating high-technological jobs, considering the safety of construction workers, complete elimination of pricy formworks, and wastage reduction [6].

Moreover, new technology might offer some extremely helpful benefits to mankind, but it comes with its own set of challenges. Despite its truly promising applications, the adoption of 3-D printed concrete (3DPC) for large-scale applications is hindered by several vital demanding situations. One of the primary limitations includes inherently low tensile capacity and ductility. This affects its structural applications, as conventional reinforcement cannot be used to withstand tension in the concrete. Another issue is that due to layer-by-layer stacking, the interface is extremely weak. Hence, for a 3DPC, a strong interfacial bond is a prerequisite for strength and durability [7].

Early studies of concrete mostly focused on adhesion, strength, and water-to-cement ratio, which dates back to 1919 [8]. But since the introduction of 3D-Printed Concrete (3DPC), interlayer behavior is growing more vital in determining structural performance. Parameters like interfacial bond strength, layer stiffness, and the time gap between successive depositions now play a significant role in controlling the mechanical response of printed elements [9]. Additionally, these interfaces are extremely vulnerable to environmental exposure, like chemical ingress, that can significantly accelerate deterioration. According to multiple studies, allowing printed layers to dry in between depositions can cause them to lose up to 50% of their interlayer capacity [7, 10]. In contrast, Austin et al. [11] observed that bond strength may increase under dry conditions, demonstrating the lack of approval in current literature and highlighting the complexity of 3DPC behavior, which is heavily influenced by mixture design and environmental conditions.

Steel is used as the primary and widely used reinforcement technique almost everywhere; however, in harsh environmental conditions, the deterioration of steel is significant, hence the steel cannot provide the necessary tensile strength in the concrete in the very long run due to corrosion. Hence, a different type of reinforcement is necessary, which can withstand the tension and does not get affected by the environmental conditions and deterioration. Composite reinforcements, such as fiber-reinforced polymers (FRPs), offer promising resistance to such deterioration mechanisms and offer enhanced mechanical properties like flexural and interlayer shear capacity [12]. The environmental effects on FRP are way less than steel reinforcement for pavement purposes, which implies a decrease in frequency for repair and maintenance [13]. Furthermore, it can serve as an appropriate substitute for steel rebar due to its lightweight, high strength, and good corrosion resistance [14]. However, the lack of knowledge and data about the durability of 3D printed reinforced concrete structures hinders the growth of these automated fabrication methods to truly offer their best for the transportation industry.

The scope of this research covers 3DPC and manually fabricated concrete with the following reinforcements: Carbon-fiber reinforced polymer (CFRP), Glass-fiber reinforced polymer (GFRP), and Steel reinforcement, to provide a comparative database for these advanced materials as reinforcements and some additional benchmarks for 3DPC. For that, the environmental deterioration mechanisms-specifically chemical ingress, are thoroughly studied, including effects on the flexural and interlayer bond strength of 3DPC elements. By exploring the response of the chemical ingress, the effect of this harsh environmental phenomenon can be better understood, and the necessary steps that can be taken in order to improve 3DPC for a durable and lasting infrastructure. Moreover, it is also anticipated that reinforcement like FRP will demonstrate better resistance to these deterioration mechanisms compared to traditional steel reinforcement, thereby improving the overall durability of 3D printed elements.

2 Literature Review

2.1 History of 3D Printing

The earliest patent resembling 3D printing dates to 1951, employing projected light to harden photosensitive materials [15]. But, for the very first time in 1981, Japanese inventor Hideo Kodama created a device using ultraviolet light to harden polymers, regarded as the first documented practical 3D printing technology [16]. 3D printing's mass popularity surged after 2009, when a key Stratasys patent expired, enabling broad commercialization and innovation-especially open-source projects like RepRap [15]. This study mentioned additive manufacturing as the third industrial revolution because of its potential to change the manufacturing market. American Society for Testing and Materials (ASTM) International Committee F42 defines additive manufacturing (AM) as a process of joining materials to make objects from the three-dimensional (3D) model data, usually layer by layer, as opposed to subtractive manufacturing methodologies [17]. 3D printers also have some footprints in the medicine sector. Personalized medicine, lower cost production, supply chain flexibility, and innovative drug delivery systems are some common areas of investigation for the 3D printed devices [18, 19]. The study outlines the classification of 3D printing types: Stereolithography (SLA), Fused deposition modeling (FDM), and Selective Laser Sintering (SLS), with technical processes, materials, and major applications in aerospace, medicine, and consumer goods with summarizing emerging techniques and limitations of each process [20]. Additive manufacturing and 3D printing have grown significantly over the years, becoming more affordable, and now encompass bioprinting and 4D printing, where the fourth dimension is time, which covers materials from polymers to metals, ceramics, and even smart materials, emphasizing innovation and mass customization.

2.2 Durability Study in 3D Printed Concrete

3D Concrete Printing has emerged as a revolutionary innovation in the construction industry and has become a game-changer for the way structures are planned and constructed. Without the use of formwork, the technology allows cementitious materials to be deposited layer by layer, creating a stack of concrete layers, which ultimately reduces the construction time and increases the material as well as the design flexibility [21]. Various technological approaches within this rapidly growing field have been presented and discussed in the literature. De Schutter et al. [22] and Bos et al. [23] addressed the potential challenges and provided some wide opportunities in this 3D printing field. Primary research has suggested that the 3D printer and 3D printed concrete can help cope with the labor shortages and reduce the wastage of materials by a significant amount [24, 25]. Rheological properties and strength of 3DPC have been a key point of attention in present-day research [4, 24, 26, 27]. Moreover, it can be seen that a good control of hydration and setting kinetics of cementitious materials is crucial to meeting complex technological requirements like pumpability, extrudability, and buildability of fresh and hardened states need to be investigated [22, 28].

Having said that, it has pros that can outweigh the cons by a significant amount. The durability and reinforcement integration with 3D printed concrete is always a matter of deep concern and a tedious task, but some innovative solutions have been suggested to reinforce the 3DPC. Strain-Hardening Cement-based Composites (SHCC) used as a 3D printed mix have higher strength compared to mold-cast SHCC specimens [29]. Another method, named as Material Deposition Method (MDM), uses a metal cable in the concrete to reinforce the printed concrete, which is very unique, and data shows that reinforcing could be possible in 3D printed mix as well [30]. Similarly, this study dictates that the use of steel as reinforcement is actually not feasible since the steel bars need to be placed within the fresh state of concrete, which disrupts the automated deposition sequence, introduces geometric discontinuities, and contradicts the layer-by-layer manufacturing principle; hence, it suggests the use of short fibers, yarns, and textiles as reinforcement [31]. Traditional reinforcement methods, such as steel bars, are challenging to implement with 3D printed concrete due to the absence of formwork and the nature of stacking the layers on top of each other. Moreover, the durability concern of 3DPC is significant when the layers are exposed to aggressive environments like environmental deterioration, such as chemical ingress, freeze-thaw, and carbonation, etc. [32].

Significant progress has been made in the field of research for 3DPC, but several gaps are still there in understanding the specific aspects of 3DPC, which indeed require some further investigation and development. Major focus is inclined towards improving the bond between the reinforcement used and 3DPC, just to make the concrete sturdy enough to hold the layers above it. Similarly, establishing the standards for testing its durability would also help with the adoption of 3DPC in its real-world applications [27, 33].

2.3 Layer-by-layer extrusion

The layer-by-layer construction technique in 3D printing is unique and at the same time a very challenging thing for all the engineers and experts, unlike conventional concrete. The concrete printing or 3D printing process uses an additive, layer-based, manufacturing technique to build complex geometrical shapes without the need for formwork, thus has a unique advantage over conventional construction methods. This is performed with contour crafting, which is based upon layer-by-layer extrusion of a cement-based paste, creating a smooth surface through the buildup of subsequent layers in Figure 1 [34]. In extrusion-based 3DPC, the requirements for fabrication are both good flowability and a layer should be able to support the weights of subsequent layers, i.e., the printed concrete needs to have a unique shear strength, material properties like thixotropy and viscosity [35, 36].

In addition, research into how vertically stacked layers affect printed materials is equally crucial because freshly prepared concrete without formwork is delicate and may exhibit various deformations in the layers that support the upper layers. Hence, there is a different set of adhesions that can vary with each layer. But, stacking layers vertically causes higher bond strength in the middle interfaces than upper and lower interfaces heightwise, according to Yu Zhang. et.al [36].

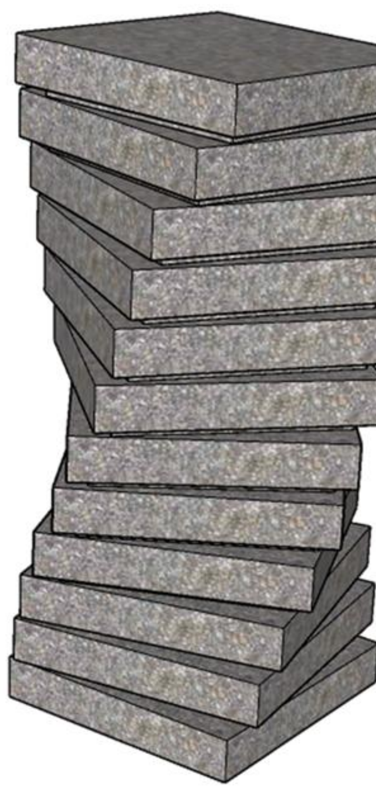

Figure 1: Layer-by-layer stacking sequence

2.4 Mix Design for 3D Printed Concrete

Mix design for the 3DPC depends on the type of printer and the strength requirements for a given task. However, a proper mix design is essential. A variety of mix designs are investigated by Zhang C. et al., suggesting various types of binding materials, namely sulphoaluminate cement and geopolymers, whose proportion is obtained from a trial-and-error procedure [26]. Some extra modifiers like Viscosity-Modifying Admixtures (VMAs) are used for providing the necessary viscosity to the mix and assisting the workability, but due to the lack of proper proportions of modifiers, which play a great role in the mix, it is a tedious process [26]. A. A Haibe studied the flexural behavior of the beams about reinforcing a 3D printed concrete beam using straight and stiff bars and shear reinforcement, providing a significant amount of relevant data to help a 3D printed concrete beam strengthen its flexural properties [37]. The study where twenty-seven different and unique mix designs for 3DPC were analyzed and worked on, and the paper helps to determine and works as a check and balance with the design mix proposed [38]. D.H. Murcia et.al. explain that textile reinforcement is used on different layers, which provides the idea of longitudinally reinforcing the 3DPC but is only confined to textiles and polymer concrete as a binder, a layout shown in Figure 2 [39].

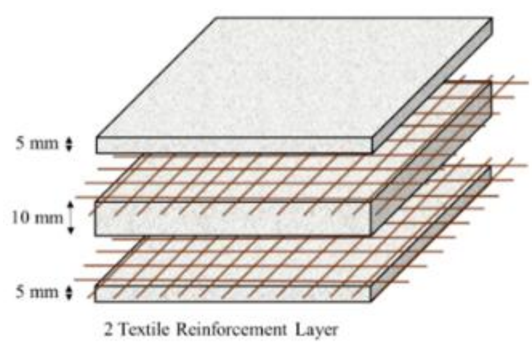

Figure 2: D.H. Murcia et.al. textile reinforcement incorporated in between the concrete

2.5 Freeze-thaw

Freeze-thaw is one of the most severe environmental degradation factors affecting concrete durability. When water penetrates through the concrete pores and freezes inside the concrete, it expands and causes degradation of mechanical properties. Cyclic freezing and thawing cause excessive damage and decrease the span of the structure [40, 41]. Experimental investigations for freeze-thaw have shown that a robust mix design can cope properly with the freezing and thawing cycles, whereas some studies suggested that glass fibers can improve the freeze-thaw resistance by resisting the crack propagation and hence achieving extended ductility before rupture [42, 43].

To study freeze-thaw mechanisms, a freeze-thaw chamber that can vary in shape and size needs to follow ASTM C666 for freezing and thawing mechanisms guidelines [44]. The freeze-thaw chamber freeze phase occurs at -18°C (0°F), and the thawing at 4°C (40°F). The phases of the freeze-thaw cycle are outlined in Figure 3. Specimens are removed every 30 ± 6 cycles.

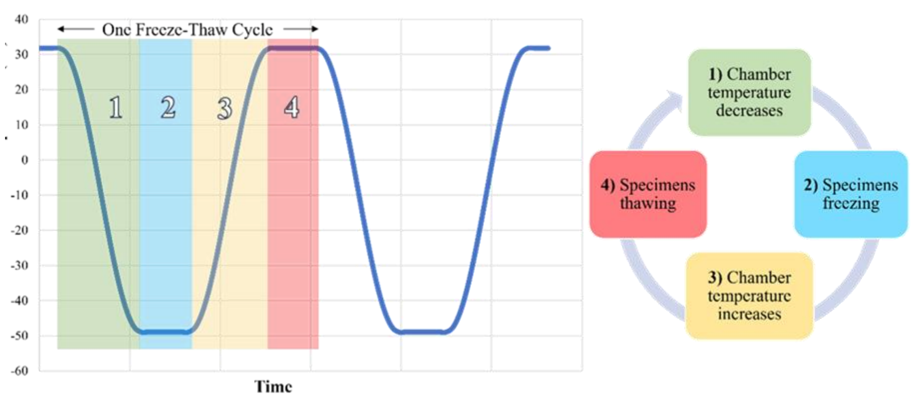

Figure 3: Freeze-thaw cycles process

2.6 Chemical Ingress

Chemical ingress, which includes chloride, sulfate, and carbonation, is one of the leading causes of durability issues in concrete. The ingress could severely affect concrete, decreasing its lifespan to a huge extent due to corrosion, expansion-cracking, and a decrease in mechanical properties, which are overall considered environmental degradation factors. In 3DPC, the layer-by-layer deposition process introduces additional vulnerabilities at the interfaces where the chemical can percolate inside and can accelerate the ingress[45, 46]. Chloride ingress is a major concern for reinforced concrete, typically for concrete to be used in a marine environment. Studies have shown that 3DPC is more susceptible to chloride penetration due to the gaps in the layer-by-layer stacking of 3D printed concrete layers [47].

Similarly, carbonation is where carbon dioxide from the atmosphere reacts with calcium hydroxide to form calcium carbonate in the cement paste, which ultimately deteriorates the concrete [48]. Moreover, sulfates are also equally responsible for the chemical to get into 3DPC. Sulfate attack occurs when the surrounding environment reacts with cement, causing extensive cracks and loss of concrete capacity. The layer acts as an easy entry point for the sulfate ions to get inside the 3DPC [49]. Significant progress in research for the chemical ingress in 3DPC has been made by Van Der Putten. et. al [47] gave some significant results on chloride penetration, but failed to cover sulfates, which are still lagging in the current study as well.

3 Hypotheses and Objectives

3.1 Hypotheses

In this study, the following hypotheses will be tested:

i. Layer-on-layer compaction-free 3D Printed elements have cold joints between layers and create an interface that may facilitate penetration of aggressive environmental elements.

ii. Environmental elements may negatively affect the flexural strength and interlayer strength of the concrete elements and the reinforcement at the interfaces.

iii. 3D printed elements with composite reinforcement, specifically FRP, may show increased resistance to deterioration mechanisms than steel reinforcement while improving flexural strength and interlayer shear capacities.

3.2 Objectives

All main objectives of this study are:

i. Assessment of durability properties of cementitious binders with multiple interlayer reinforcement to mitigate the deterioration caused by aggressive environments and the development of high ductility 3D printed concrete elements for transportation systems.

ii. Preparation of a comparison data sheet between the cementitious binder with successive layers representing 3D printed elements and reinforced cementitious binder with reinforcement incorporated at the interface between successive layers and providing microscopic analysis of failure surfaces.

iii. Suggesting the ideal reinforcement for the 3D printed elements from the data sheet.

4 Approach and Scope of Work

In this study, the durability of 3DPC under the environmental degradation mechanisms of chemical ingress and freeze-thaw cycles is investigated in comparison with manually fabricated concrete, with the flowchart in Figure 4. The approach concentrates on material selection, fabrication for both manual and 3D printed elements, durability assessment, microscopic analysis of surfaces, and preparation of a comparison data sheet.

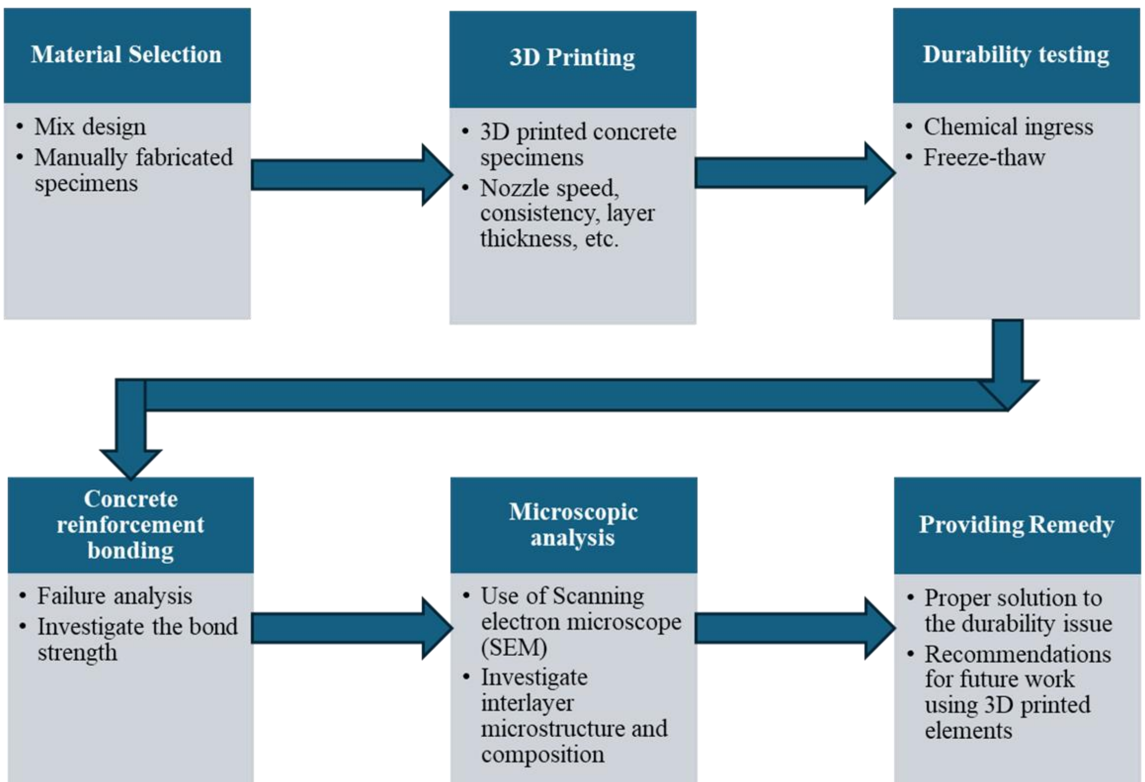

Figure 4: Approach of work

The scope of the work covers all the aspects of the experimental procedure, like the fabrication of 3D printed specimens and their long-term performance under given environmental exposure. Also, modifications to the mix design are needed to minimize the chemical ingress and boost the freeze-thaw resistance of the concrete. The work shall be a benchmark for applications of a 3D printer for large-scale printed elements in transportation, such as bridges, culverts, etc., and should work as a guideline for using 3DPC in the real world, considering all the environmental aspects. The test matrix is provided in Figure 5.

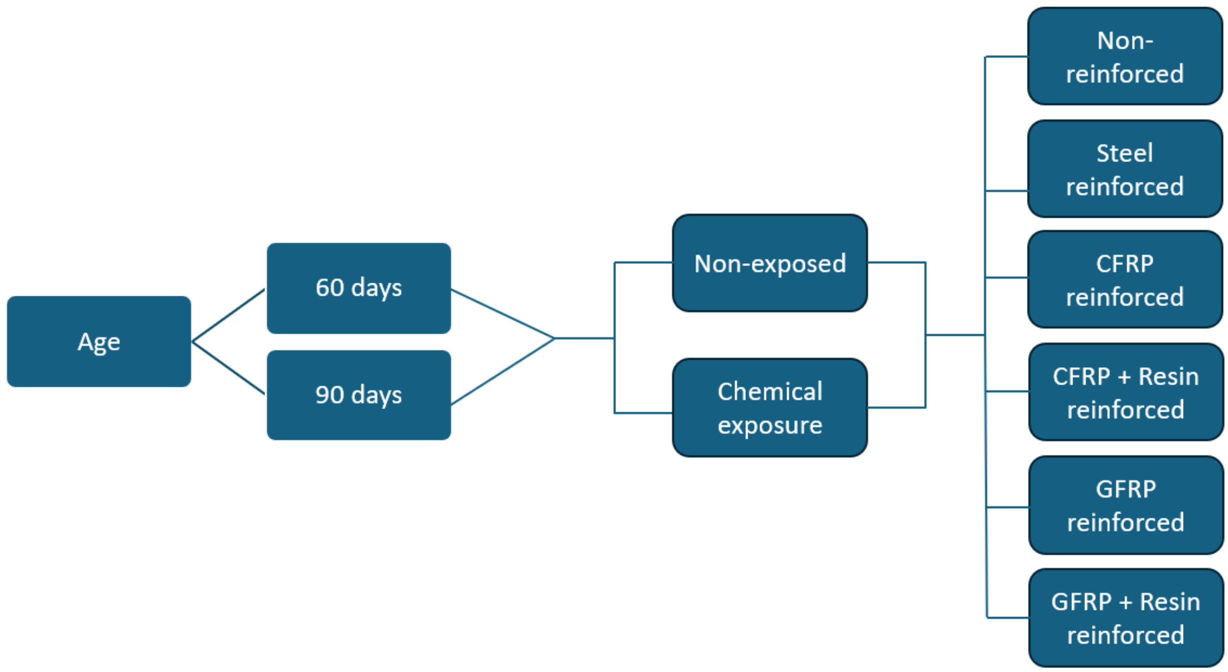

Figure 5: Test matrix of specimens

5 Phase A: Manual Fabrication

5.1 Mix Design

Mix design plays a vital role in assuring the ability to gain proper tensile and overall structural performance. An ideal mix design should possess proper printability, possessing a rheological profile that allows smooth extrusion without segregation or clogging. The mix should be durable enough to restrain the ingress of chemicals through it. Chlorides, sulfates, and carbon dioxide are highly permeable compounds that tend to attack and ultimately deteriorate the mix. Incorporating additives like fibers and reinforcement can contribute to the ductility and tensile capacity. Mix should also be able to handle the freezing and thawing mechanisms. The particle size distribution for fine aggregates for the mix selected is in Figure 6 which has a nominal aggregate size of 2.36mm. The water/binder ratio of the mix design for the study is 0.28. The constituents of the mix design are in Table 1:

Table 1: Components of mix design for Phase A

Material	Quantity
Cement	546 kg/m^3
Fly Ash	156 kg/m^3
Silica Fume	78 kg/m^3
Sand	1171 kg/m^3
Water	219 kg/m^3
High-range Water Reducer (HRWR)	8.2 kg/m^3

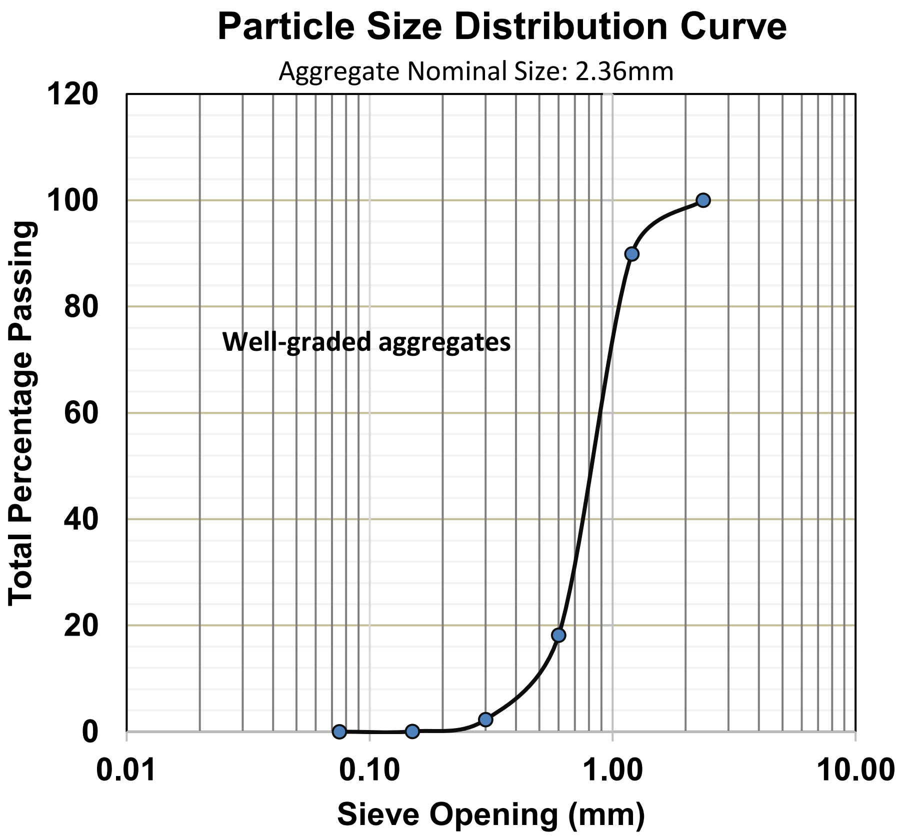

Figure 6: Particle size distribution curve for sand

5.2 Reinforcements

The reinforcement plays a significant role in enhancing the performance of the mix. It helps to assist the tensile strength and ductility, addressing the brittle nature of the concrete. For the 3DPC, the placement of reinforcement is a very tedious task, particularly on the interface, where a weaker bond can create deterioration. The reinforcements used in this study are described in the following sections.

5.2.1 Carbon Fiber-Reinforced Polymer (CFRP)

The CFRP fabric is made up of carbon fiber, which is embedded in a polymer matrix. The CFRP fabric offers a high strength-to-weight ratio, corrosion resistance, is extremely lightweight, and highly durable. The CFRP Fabric in Figure 7 is more popular in the current context due to its wide range of applications in reinforcing the 3DPC. This ultimately offers a very strong alternative to traditional steel reinforcement.

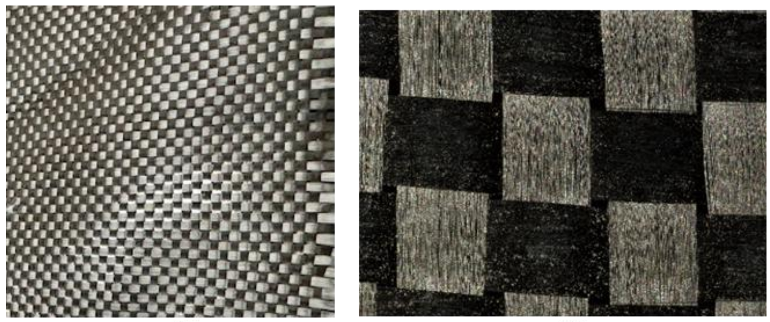

(a) (b)

Figure 7: (a) CFRP Fabric, (b) Microscopic 40X image for CFRP Fabric

5.2.2 Glass Fiber-Reinforced Polymer (GFRP)

The GFRP fabric is made up of glass fibers, which are properly embedded in a polymer matrix, that can offer an alternative as well as extreme resistance to corrosion. It has wide applicability due to its lightweight and cost-efficient nature. In 3DPC, GFRP fabric in Figure 8. It is a perfectly suited candidate for reinforcement in aggressive environments where traditional steel reinforcement might face durability issues.

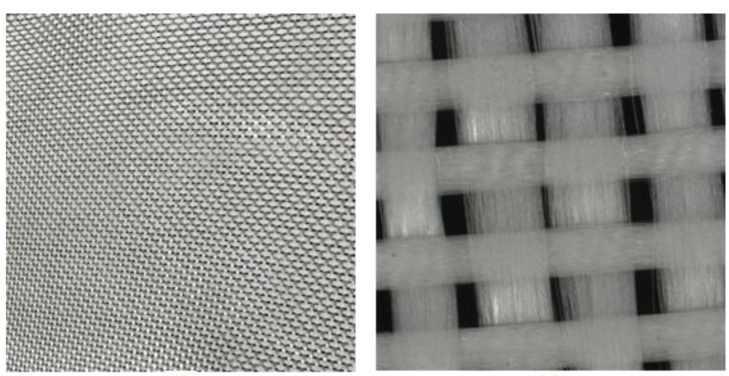

(a) (b)

Figure 8: (a) GFRP Fabric, (b) Microscopic 40X image for GFRP Fabric

5.2.3 Steel Reinforcement

Steel mesh is a conventional reinforcement technique composed of interconnected steel wires or bars, forming a grid-like pattern. The wide range of steel in construction is due to its high tensile strength, availability, and cost-effectiveness. In this study, the stainless steel 120 mesh with an aperture of approximately 0.13mm and a wire diameter of 0.09mm is shown in Figure 9 is introduced to prepare a comparable dataset and to know how the environmental degradation affects the actual concrete and steel that is used.

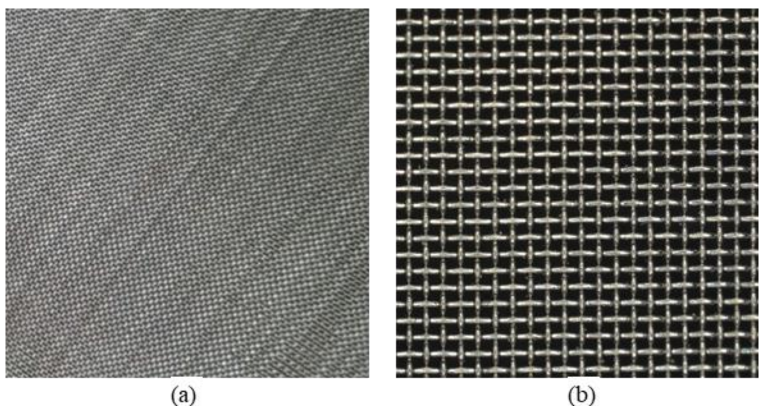

Figure 9: (a) Steel Mesh, (b) Microscopic 40X image for Steel Mesh

Microscopic analysis of each type of reinforcement was performed to investigate the gap sizes in the fibers for CFRP, GFRP, and steel reinforcement. For that, the Keyence VHX-7000 ultramicroscope at the Samuel Roberts Noble Microscopy Lab (SRMNL) in the University of Oklahoma was used to obtain the images on Figure 10 ensuring that the materials that are to be compared are of similar shape and size, given that not all the gaps are of the same size, but ensuring the best possible comparison of an apple to an apple. This helps to provide similar bonding conditions between the reinforcement and concrete, and hence, a reasonable comparison shall come out of it. The red gridlines are the guidelines for measuring the length and breadth of the gap for the reinforcement that was investigated under high magnification of 300X.

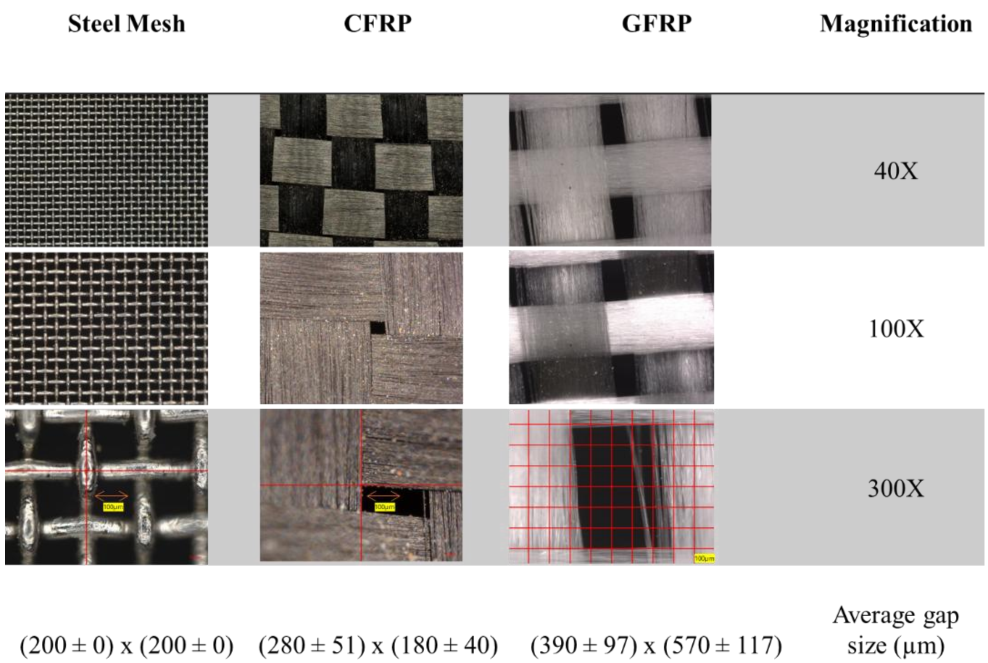

Figure 10: Microscopic images of reinforcement used along with fibers gap size

5.3 Flow and Setting Time

Flow or standard test method for flow of hydraulic cement mortar (ASTM C1437) is a standard test method used to determine the workability or consistency of the mix that does not have coarse aggregates. It evaluates the flow by assessing how the mix spreads on the flow table and determining the percentage of the diameter of the mix that flowed to the initial diameter of the table. This test is useful for quality control and ensuring the mix meets the desired specifications for applications[50]. Specific procedures include the mold, which is filled in two layers followed by 20 tamps each, and then the table is dropped 25 times under 15 seconds, and then the mold is removed. The mix flows into the table, and hence, the flow of the mix in a measure of diameter is measured as a spread on the table. Flow was conducted in each batch to get a consistent mix, whereas the setting time test was conducted once. The flow table is shown in Figure 11.

Figure 11: Flow table

Setting time or Standard test methods for time of setting of hydraulic cement by Vicat Needle (ASTM C191-18a) is a standard test method used to determine the time of setting of hydraulic cement. This test measures the rate at which cement starts to set, which is very crucial for workability and construction timing. Specific standard procedures involve filling the mold for Vicat's apparatus, and a 1mm diameter needle is lowered, and the penetration is recorded every 15 minutes. Vicat's apparatus is shown in Figure 12. Final set time is achieved when the needle does not make any penetration and leaves a mark on the surface[51].

Figure 12: Vicat's Setting time apparatus

5.4 Preparation of specimens for Compressive Strength Test Method

The standard test method for compressive strength of hydraulic cement mortars using 2-in or 50-mm cube specimens is to determine the compressive strength of hydraulic cement mortars.

The test is critical for evaluating the strength properties of cementitious materials used in construction and is often used as a benchmark for material performance. Standard procedures include cubes of molds 50mm x 50mm, where the mix is placed in two layers of compaction 16 times each, as shown in Figure 13. The cubes are demolded after 24 hours and are cured under water for 7, 14, and 28 days, respectively [52].

Figure 13: 50mm x 50mm cementitious cube preparation

5.5 Compressive Strength Test

As mentioned above, cementitious cubes that are cured for 7, 14, or 28 days are placed on the Forney compression testing machine, and load is applied until failure. This test is based on ASTM C109. The ramp rate used is: 0.206 MPa/sec, and the preload applied is 1.112 kN, as shown in Figure 14.

$$\text{Compressive Strength} = \frac{\text{Maximum Load (N)}}{\text{Cross Sectional Area } (\text{mm}^2)}$$

Figure 14: Forney compression testing for cubes

5.6 Fabrication of Specimens by Manual Fabrication (Non-reinforced)

Manually fabricated specimens of dimensions 4-in x 4-in x 15-in were cast using wooden formworks. For the non-reinforced, the fabrication was performed similarly compared with the reinforced ones. The beam size used was fixed according to the freeze-thaw and the chemical ingress chamber's area restrictions. The non-reinforced specimen can be seen in Figure 15.

Figure 15: Non-reinforced manual fabrication

5.7 Fabrication of Specimens by Manual Fabrication (Reinforcement)

Manually fabricated specimens of dimensions 4-in x 4-in x 15-in were cast, and the reinforcement was placed 1-in from the top and bottom faces. The beam size used was fixed according to the freeze-thaw and the chemical ingress chamber's area restrictions. The mold and fabrication is shown in Figure 16.

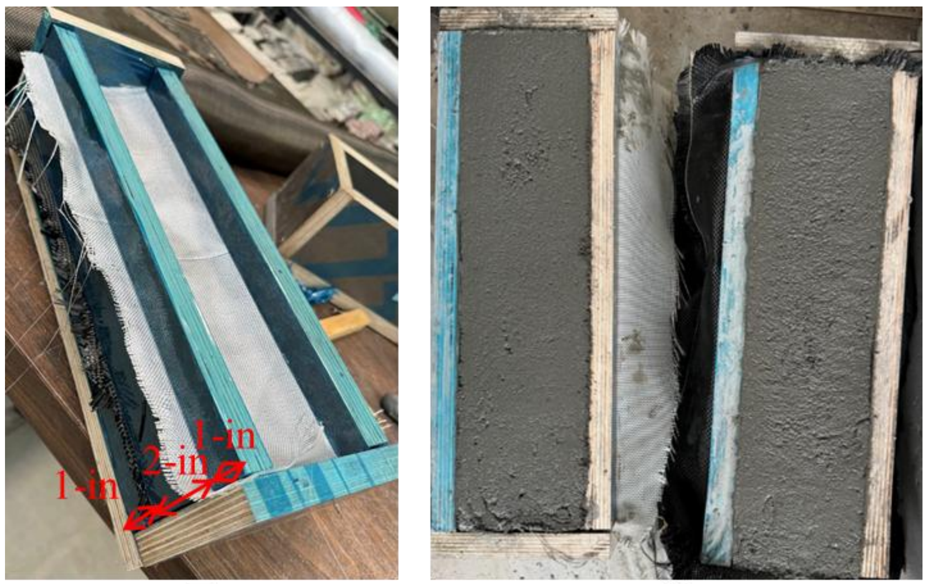

(a) (b)

Figure 16: (a) Mold with interlayer reinforcement placement, (b) Reinforced GFRP (left) and CFRP (right) fabrication

5.7.1 CFRP

CFRP reinforced specimens are fabricated. The first layer of concrete was added in the wooden mold, where the height portion was cut into 1-in from top and bottom. The first 1-in layer was filled with concrete and compacted. Then, manually, the CFRP fabric was placed, and another layer of wooden piece was fixed, which was also filled with concrete, and the fabric was again fixed. The top layer compaction, after that, concludes with the fabrication. This can be seen in Figure 17.

Figure 17: CFRP reinforced manual fabrication

5.7.2 GFRP

GFRP reinforced specimens were also fabricated in the same way. The first layer of concrete was added in the wooden mold, where the height portion was cut into 1-in from top and bottom. The first 1-in layer was filled with concrete and compacted. Then, manually, the GFRP fabric was placed, and another layer of wooden piece was fixed, which was also filled with concrete, and the fabric was again fixed. The top layer compaction, after that, concludes with the fabrication. This can be seen in Figure 18.

Figure 18: GFRP reinforced manual fabrication

5.7.3 Steel reinforcement

Steel-reinforced specimens are also fabricated in the same way. The first layer of concrete was added in the wooden mold, where the height portion was cut into 1-in from top and bottom. The first 1-in layer was filled with concrete and compacted. Then, manually, the steel fabric was placed, and another layer of wooden pieces as a part of formwork was fixed, which was also filled with concrete, and the fabric was again fixed. The top layer compaction, after that, concludes with the fabrication. This can be seen in Figure 19.

Figure 19: Steel reinforced manual fabrication

5.8 Fabrication of Specimens by Manual Fabrication (Reinforcement with resin)

5.8.1 CFRP with Resin

CFRP reinforced with resin specimens were also fabricated in the same way. The first layer of concrete was added in the wooden mold, where the height portion was cut into 1-in from top and bottom. The first 1-in layer was filled with concrete and compacted. Then, manually, the CFRP fabric dipped in resin was placed, and another layer of wooden piece as a part of formwork was fixed, which was also filled with concrete, and the fabric was again fixed. The top layer compaction, after that, concludes with the fabrication. This can be seen in Figure 20.

a) b)

Figure 20: (a) CFRP reinforcement dipped in resin+hardener, (b) Reinforcement placed in the beam

5.8.2 GFRP with Resin

GFRP reinforced with resin specimens were also fabricated in the same way. The first layer of concrete was added in the wooden mold, where the height portion was cut into 1-in from top and bottom. The first 1-in layer was filled with concrete and compacted. Then, manually, the GFRP fabric dipped in resin was placed, and another layer of wooden piece as a part of formwork was fixed, which was also filled with concrete, and the fabric was again fixed. The top layer compaction, after that, concludes with the fabrication. This can be seen in Figure 21.

a) b)

Figure 21: (a) CFRP reinforcement dipped in resin+hardener, (b) Reinforcement placed in beam

5.9 Preliminary Flexural Strength Test (Four-point bending)

Manually fabricated 28-day cured beam specimens are tested in a Forney compression testing machine using a 4-point bending test with a ramp rate of 0.0173 MPa/sec and a preload of 2.224 kN. A load was applied until the specimens failed in flexure, as shown in Figure 22. The flexural testing was performed to check whether the bond between the concrete and the reinforcement is strong enough or not.

(a) (b)

Figure 22: (a) Forney flexural testing setup, (b) 4-point bending test setup

5.10 Flexural tests (Three-point bending)

When all the manually fabricated specimens were cured and aged in respective chemical ingress or freeze-thaw chambers, the specimens were taken out and placed under a 250 kN MTS 810 hydraulic frame using LVDT sensors at a displacement of 1mm/min on the mid span, which shall provide the necessary deflection data with load following ASTM C580 and ASTM C78. The setup is shown below in Figure 23. The load was applied until the specimen's failure. Failure surfaces were thoroughly studied.

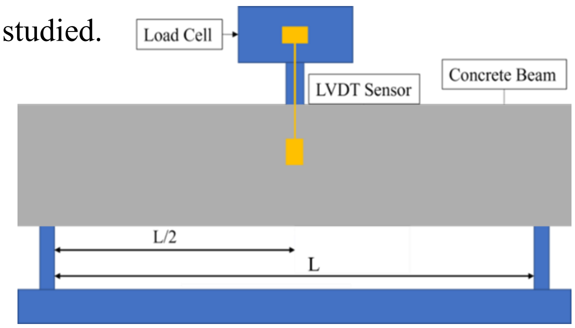

Figure 23: Three-point bending test setup on 250 kN MTS 810 hydraulic frame

5.11 Specimen Deterioration

5.11.1 Chemical Ingress

A chemical ingress chamber is created with water and 6% NaCl solution. Sulfuric acid is added regularly to maintain a pH less than or equal to 2, as shown in Figure 24 . The 14-day cured beam specimens are subsequently placed in the chamber, and ingress is measured at 30-day intervals for 90 days, taking pictures of specimens and comparing them with the 0-day ones.

(a) (b)

Figure 24: (a) Chemical ingress chamber, (b) pH of chamber maintained less than 2

5.11.2 Freeze-thaw

The 14-day cured beam specimens are placed in a freeze-thaw chamber (ASTM 666)[44]. Resonant frequency and dynamic modulus of elasticity are directly correlated. Over the cycles, the dynamic modulus of elasticity decreases as the cracks reduce the concrete's ability to resist deformation, hence the stiffness decreases, the material becomes less elastic and more brittle, leading to a drop in resonant frequency. The freeze-thaw chamber freeze phase occurs at -18 °C (0 °F), and the thawing occurs at 4 °C (40 °F). The freeze-thaw chamber cycle is shown in Figure 25. Specimens are removed every 30 ± 6 cycles. The test is stopped when the relative dynamic modulus of elasticity at given cycle 'n' is obtained when the frequency at 'n' cycles is 60-70% of its initial value. To measure the frequency, accelerometers measure the vibrational response of concrete, which is embedded in the device named Emodumeter.

(a) (b)

Figure 25: (a) Freeze-thaw chamber, (b) Emodumeter

5.12 Testing and results

5.12.1 Flow, Setting Time, and Compressive Strength

The flow of the mix was less than 1% when measured by comparing the diameter after 25 blows with the initial diameter, which seems to depict that the mix had almost zero flowability. Similarly, Vicat's initial setting time of the mix obtained was 140 minutes. This implies that the time for printing and cleaning should be under 140 minutes. The 28-day compressive strength obtained for 2-in x 2-in, or 50-mm x 50-mm cubes was 80.0 ± 1.5 MPa. These tests and their results are in Figure 26 and in Table 2. The 7- and 28-day compressive strength data were analyzed, and ultimately, 14-day compressive strength data were chosen instead of 28-day, as the beams' curing time, since the strength was comparable, having benefited from an extra 14 days, which is shown in Figure 27.

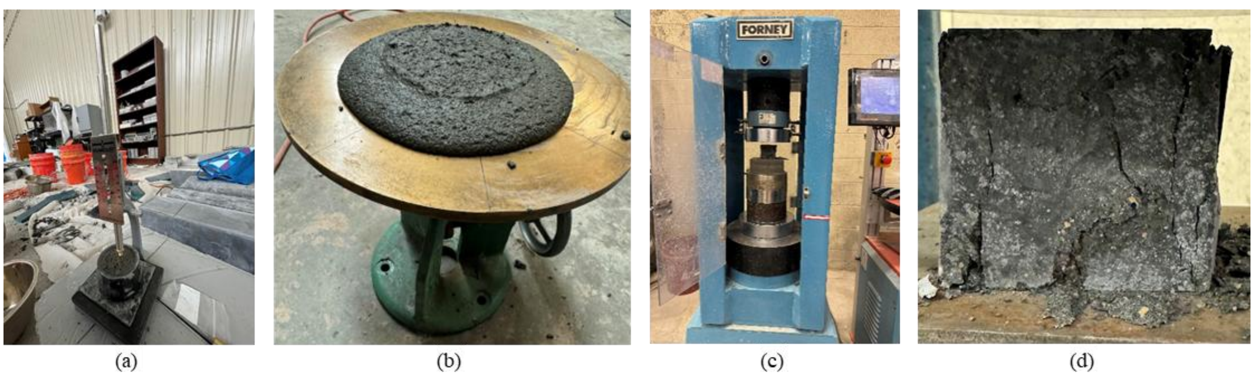

Figure 26: (a) Vicat's needle (ASTM C191-18a), (b) Flow table test, (c) Forney compression testing for 2-in x 2-in cubes, (d) Failed cube specimen

Table 2: Compressive Strength data

Curing (days)	**Compressive Strength (MPa)**
7	59.4 ± 0.4
14	67.1 ± 0.1
28	80.0 ± 1.5

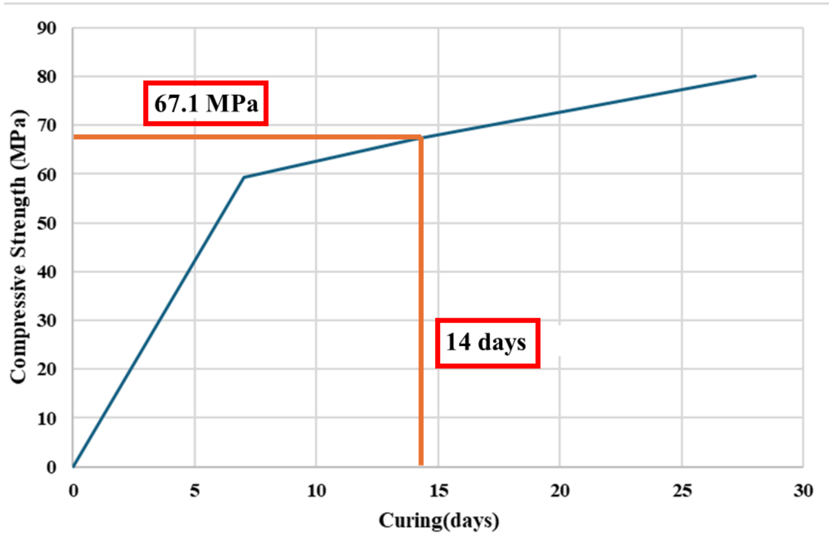

Figure 27: Compressive Strength vs Curing time

5.12.2 Preliminary Flexural Strength – 0-day exposure

One of each manually fabricated beam specimen, having each type of reinforcement, was tested in flexure as 4-point bending after curing to understand the 0-day exposure conditions for flexural strength. Results showed that each type of reinforcement aided the integrity of the beam compared to the unreinforced beam's performance.

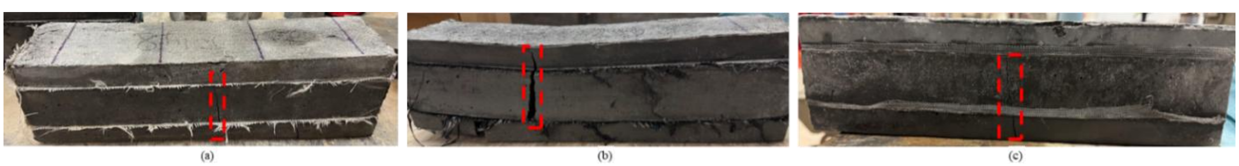

Figure 28: (a) 0-day exposed GFRP beam after failure, (b) 0-day exposed CFRP beam after failure, (c) 0-day exposed Steel beam after failure

At the failure surface of GFRP and CFRP, the crack is penetrating from top to all the way to the very bottom, which implies that the bond between the concrete and the reinforcement is good and strong in Figure 28.

5.12.3 Deterioration Mechanisms

5.12.3.1 Chemical Ingress

Beam specimens are progressively deteriorated due to the chemical getting inside the specimens through the interface. Similarly, the bonding between the reinforcement and the concrete due to the chemical ingress is getting weaker in Figure 29. The deterioration was recorded after 90 days of ingress. This is proven by the degradation of reinforcement on the external side and the formation of cracks on the specimen, which are getting larger when observed.

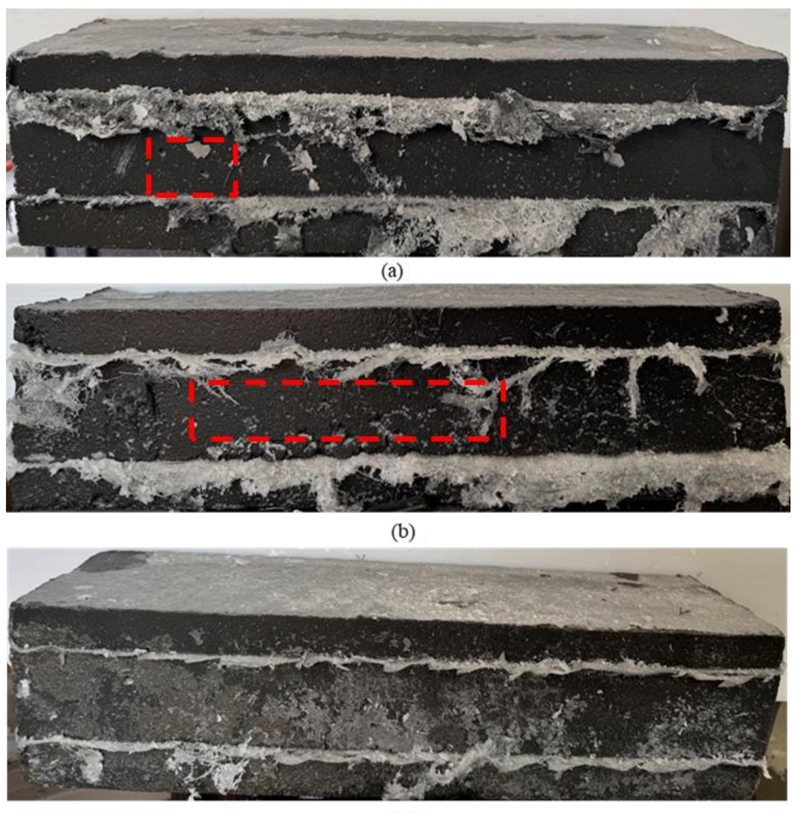

Figure 29: Beam deterioration due to chemical ingress after 90 days (a) CFRP, (b) GFRP, (c) Steel reinforcement

5.12.3.2 Freeze-thaw

Beam specimens were progressively deteriorated due to freeze-thaw cycles. Bonding between the reinforcement and the concrete due to freeze-thaw action was getting weak, which was followed by cracks that could be seen on the surface and were getting wider. The red rectangles in the Figure 30 below show the deterioration of the specimens and the cracks being developed. Freeze-thaw deterioration was determined from the emodumeter by plotting resonant frequency vs the number of freeze-thaw cycles. CFRP has shown a downward trend and again rose sharply afterwards. Steel has always been on top and rising. However, from 150 to 200 cycles, both CFRP and GFRP have shown a rise in frequency. The specimens were intact after 300 cycles of freeze-thaw for CFRP, GFRP, and Steel reinforcement. The reason for the upward trend is the mix design that was robust enough not to let the resonant frequency fall. The freeze-thaw cycles with resonant frequency can be seen in Figure 31.

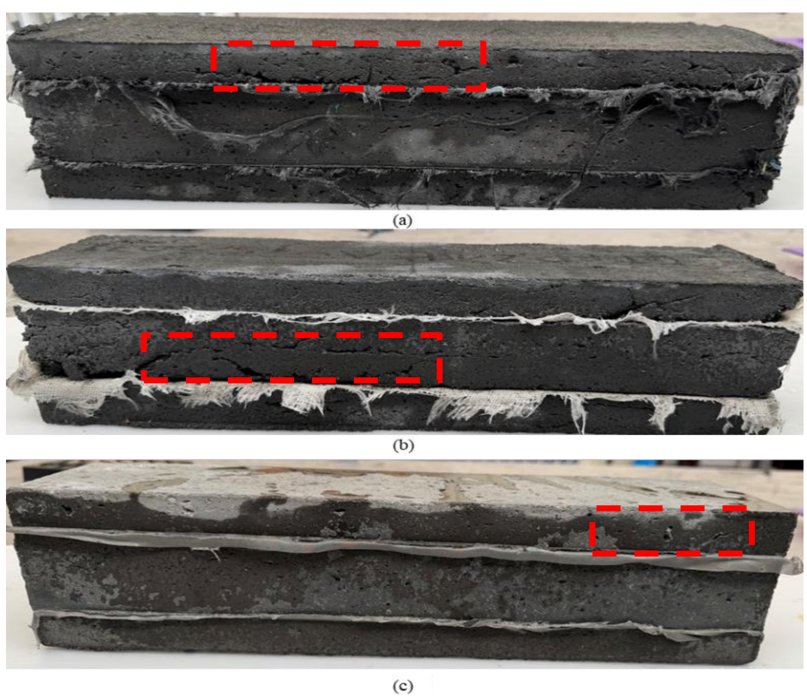

Figure 30: Beam deterioration at 300 freeze-thaw cycles for (a) CFRP, (b) GFRP, (c) 150 cycles for Steel reinforcement

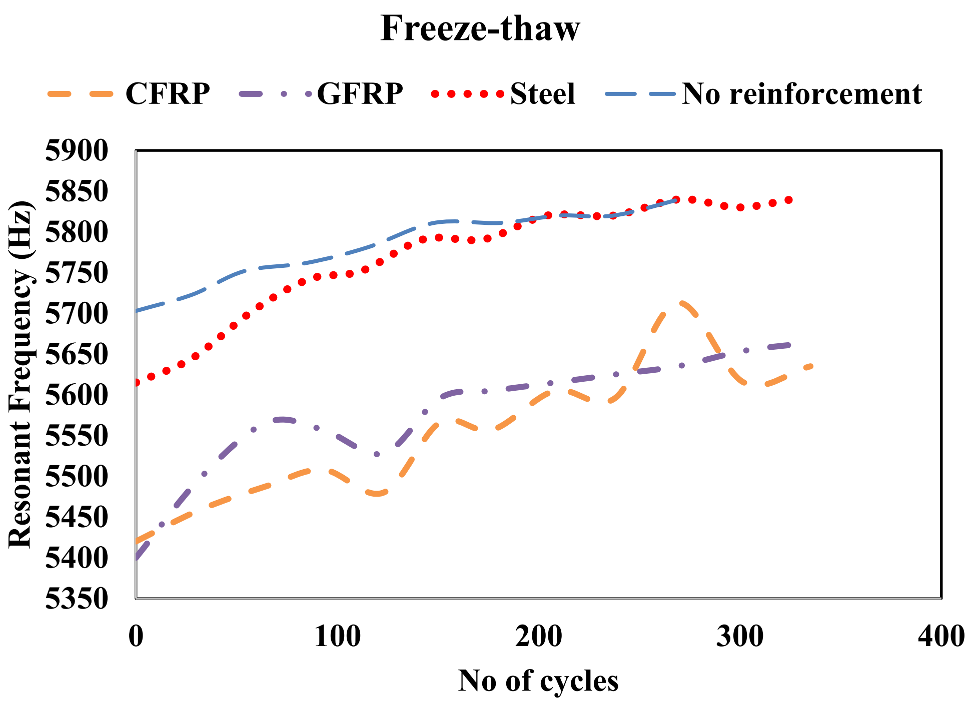

Figure 31: Resonant Frequency vs No of Freeze-thaw cycles until 300 cycles

5.12.4 Load vs Displacement

Load vs MTS displacement was plotted after specimens were tested under an MTS frame for each manually fabricated beam with freeze-thaw and chemically ingressed specimens. Each of the reinforced freeze-thaw and chemically ingressed specimens had a progressive failure mechanism rather than catastrophic collapse failure, except for the non-reinforced ones. The load was carried successively by different layers until total rupture of the specimen. Figure 32 shows the freeze-thaw-exposed CFRP reinforced specimen after 300 cycles as a demonstration of the crack propagation mechanism. Each crack in Figure 32 that had been initiated was traced through a video camera, with overall failure shown next to the plot. The first crack observed was around 5200 N at 0.8 mm displacement; however, the specimen remained intact and was able to distribute load, but at a reduced level. When the second layer failed at around 2 mm, the specimen lost more of its capacity until the final drop, which led to rupture. Fiber-reinforced polymers aided ductility (nearly 5 mm displacement) and provided subsequent warnings before failure, rather than sudden brittle failure. This can be seen in Figure 32.

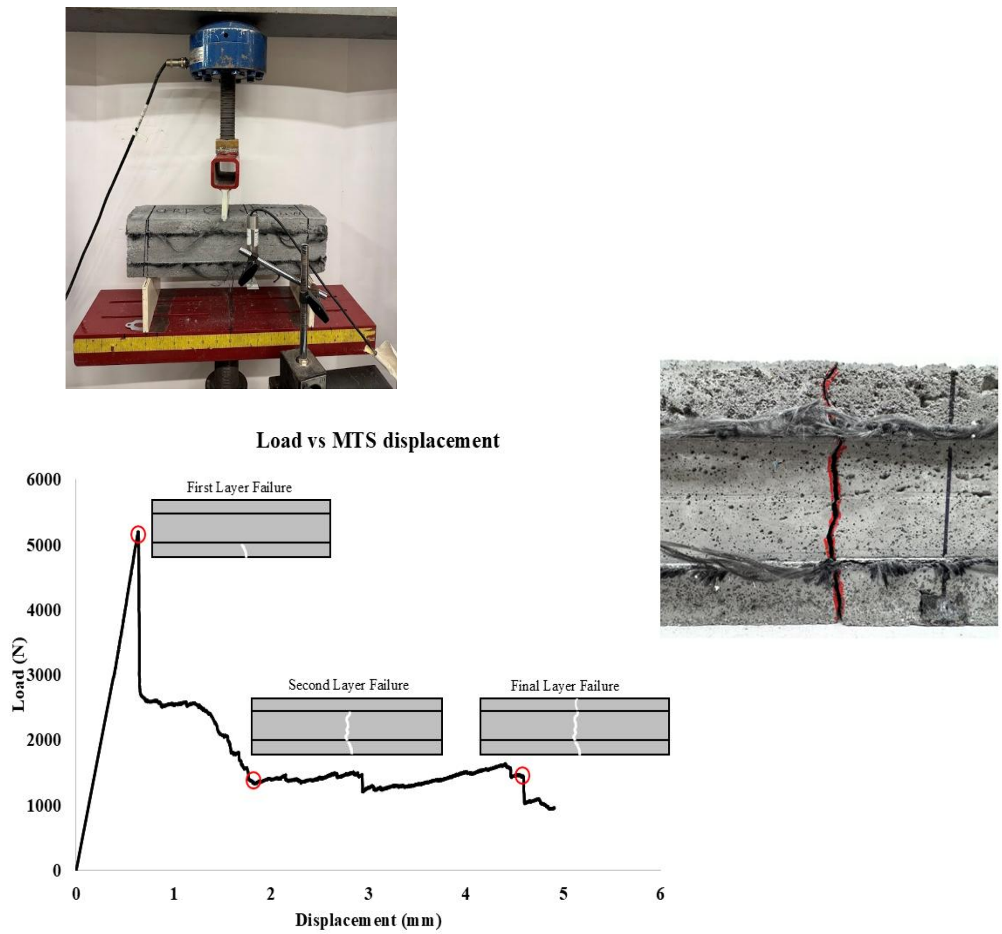

Figure 32: Load vs MTS Displacement of CFRP reinforced specimen after freeze-thaw exposure

The CFRP specimen load-displacement behavior has significant degradation due to environmental exposure. The unexposed specimens have the highest initial peak load of ~ 6 kN and then sustain a residual capacity of ~ 1.8 kN, indicating relatively intact matrix adhesion at first crack. The chemical ingressed specimen also exhibited the same peak of ~ 6 kN, and secondary recovery rose to ~ 6.2 kN and gradually decreased to ~ 2 kN. Moreover, the freeze-thawed specimen acted the weakest with a peak load of ~ 5 kN, with steep degradation and finally attaining a stable ductile failure. Figure 33 shows the load vs displacement for CFRP reinforced specimens.

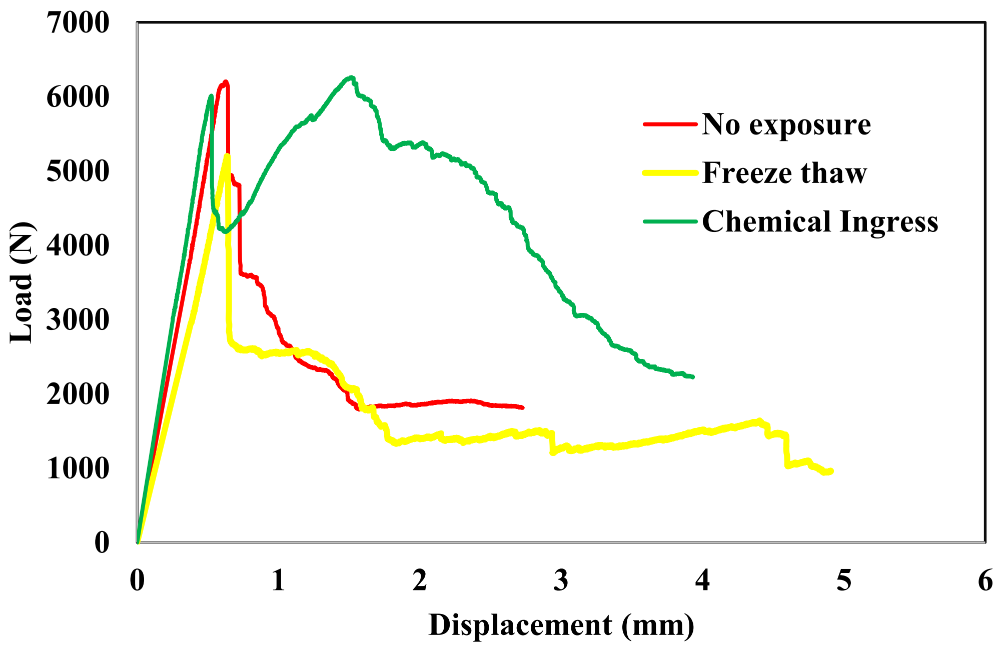

Figure 33: CFRP reinforced specimen testing after freeze-thaw, chemical ingress and no exposure

The steel-reinforced specimens' load-displacement response shows the different impacts of environmental exposures. Even after continuous freezing and thawing, freeze-thaw specimens performed exceptionally well with the highest peak load (~10 kN), provided improved initial stiffness and strength; however, they suffered a sharp drop and reduced ductility. The chemically exposed specimen performed the worst, demonstrating the severe bond degradation at the steel-concrete interface due to chemical attack. Moreover, the unexposed specimen performed exceptionally well, achieving a peak of (~7.8 kN) while being the most ductile among its counterparts (displacement ~ 6 mm) with residual strength of around 2.5 kN. Figure 34 shows the crack propagation for freeze-thawed specimen, whereas Figure 35 shows the Load vs displacement of steel-reinforced specimens.

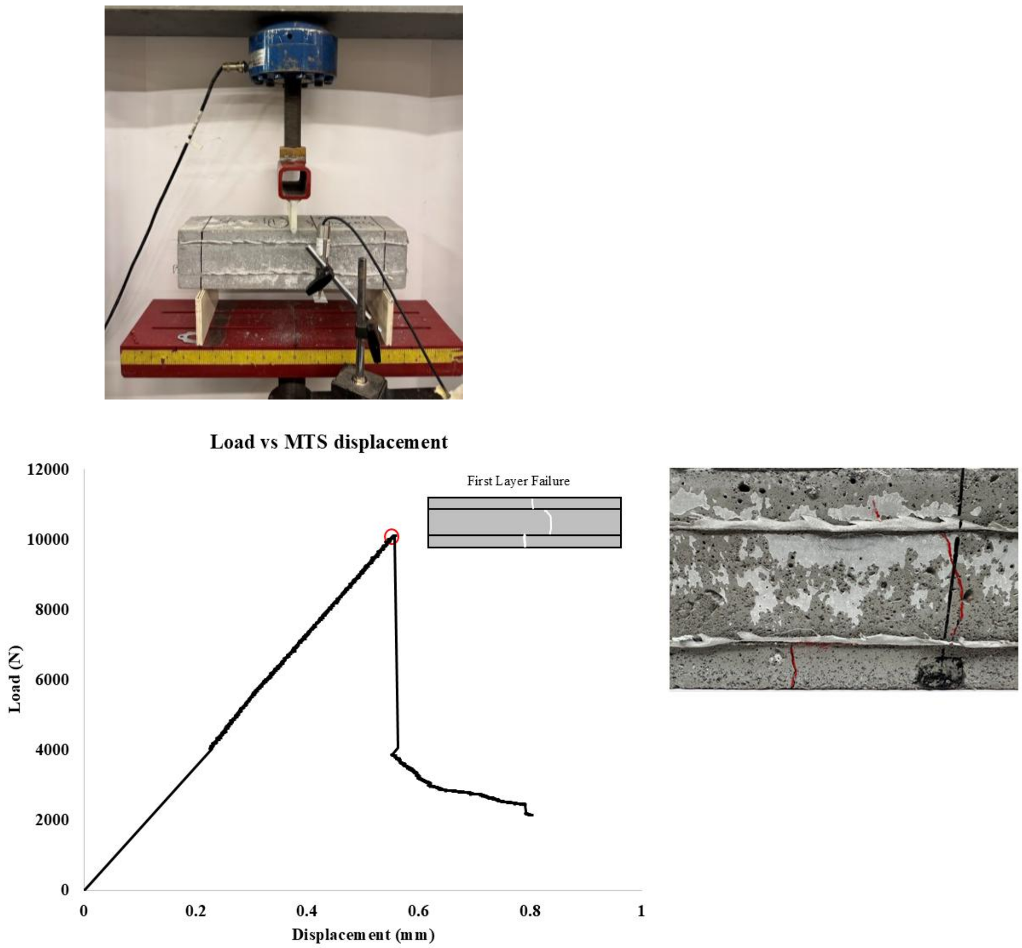

Figure 34: Load vs Displacement of Steel reinforced specimen after freeze-thaw exposure

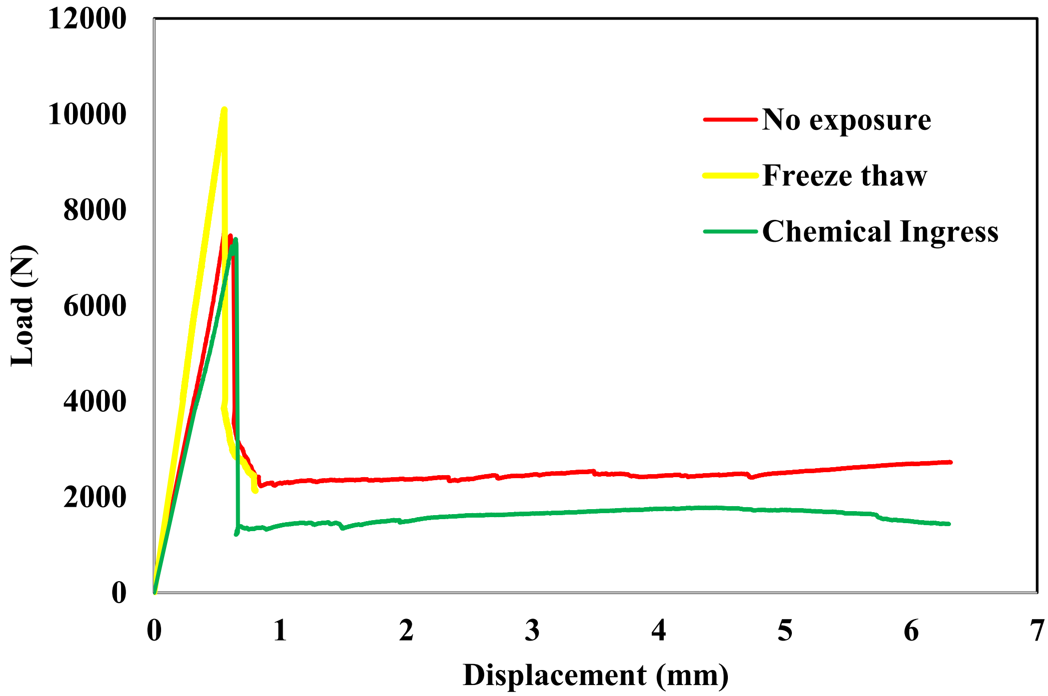

Figure 35: Steel reinforced specimen testing after freeze-thaw, chemical ingress and no exposure

The load-displacement response of GFRP specimens reflects the profound effects of environmental exposures on structural performance. Non-exposed sample recorded the highest peak ~ 5.5 kN, but post-peak behavior significantly dropped and remained consistent until the displacement reached ~ 3mm. The chemically ingressed sample registered a lower peak of ~ 2.5 kN, showing a partial recovery followed by a sharp fall to near-zero capacity: weakening bonding and successive cracking under chemical attack. The freeze-thaw specimens registered the lowest initial peak ~ 3.5 kN but had a long post-peak tail with residual strength of ~ 0.5 kN with up to a displacement of ~ 6 mm, which suggests the GFRP reinforced freeze-thawed specimen acted the weakest among all the specimens. Figure 36 describes the crack propagation of the freeze-thawed specimen, where cracks were traced at each layer, whereas Figure 37 shows load vs displacement for GFRP reinforced specimens.

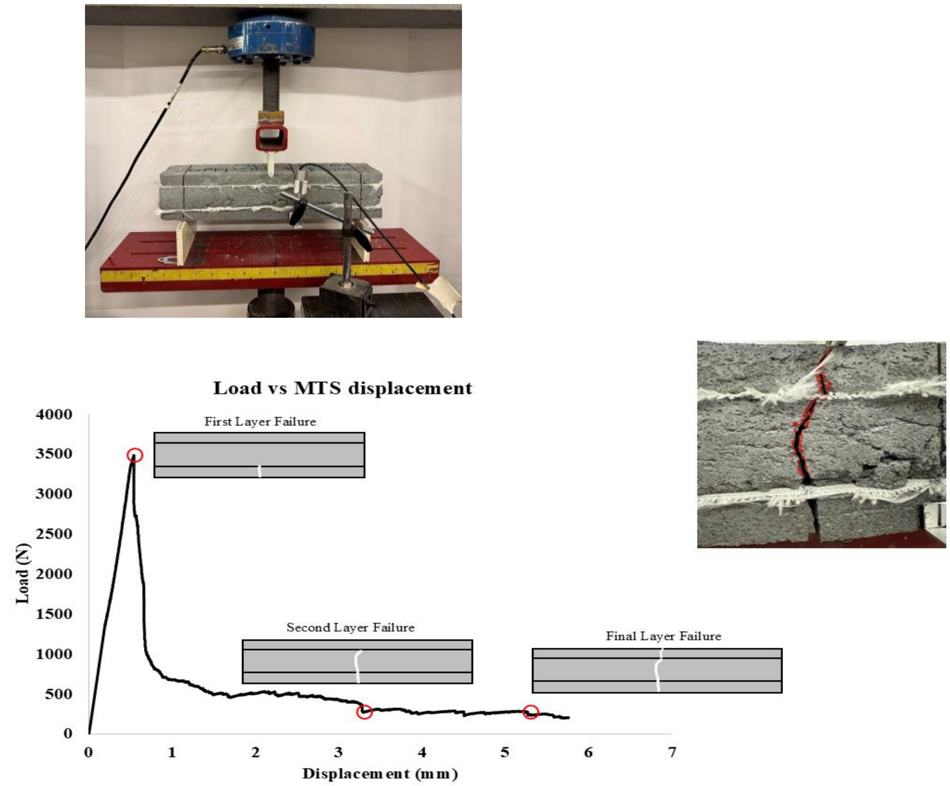

Figure 36: Load vs Displacement of GFRP-reinforced specimen after freeze-thaw exposure

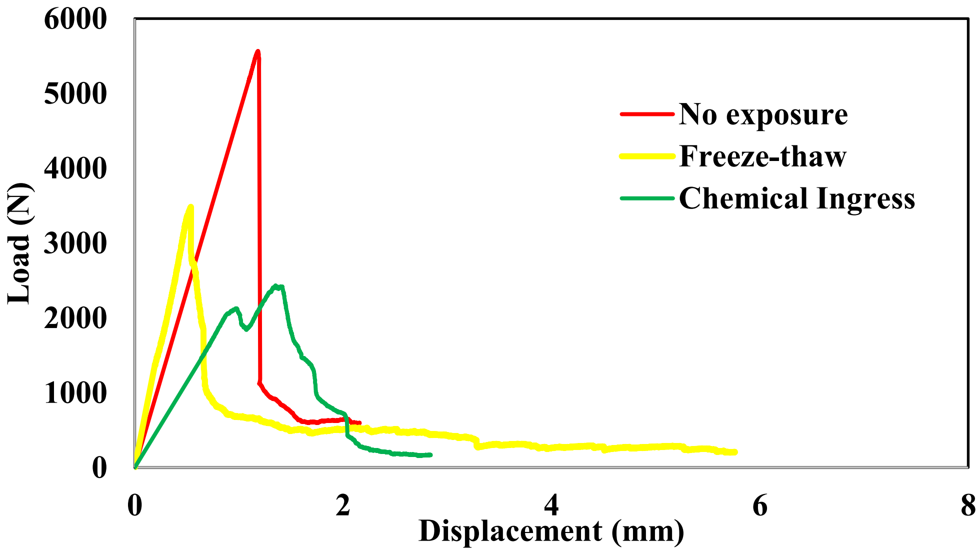

Figure 37: GFRP reinforced specimen testing after freeze-thaw, chemical ingress and no exposure

Figure *38* shows the load-displacement behavior of CFRP + resin reinforced manual specimens under two different conditions: Chemical ingress and non-exposed ones. The chemically exposed specimen rose more sharply at the very start, indicating higher initial stiffness, which could be from the densification near the surface. The peak load observed was around 20 kN compared to the unexposed ones that were around 15 kN. The post-peak behavior was similar for both specimens as the specimen subjected to chemical ingress dropped sharply after the peak; however, it again rose, which gives the information that the drop and rise were stepwise. The non-exposed specimen showed a more gradual drop and multiple smaller peaks, implying progressive damage and better ductility. Even though the specimen subjected to chemical ingress had increased load capacity, the failure was somewhat brittle and less ductile compared to the non-exposed one. Freeze-thaw was not carried out for the CFRP + resin reinforced specimen due to some internal machine issues, and the frequency and dynamic modulus did not decrease over the time taken to reach 300 cycles for the former specimens that were tested.

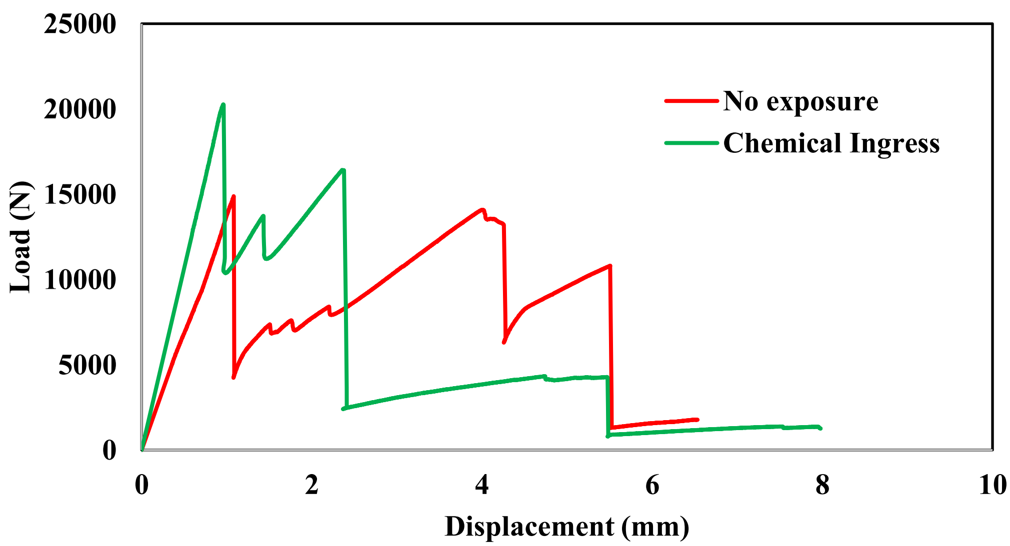

Figure 38: CFRP+ Resin reinforced specimen testing after chemical ingress and no exposure

Figure 39 shows load-displacement behavior of GFRP + resin reinforced manual specimens under two different conditions: Chemical ingress and non-exposed ones. The specimen placed in the chemical ingress chamber showed a very steep initial rise that went all the way to 12.5 kN; however, it dropped immediately after the peak, and a brittle behavior was observed. On the other hand, the non-exposed specimen had a smaller peak load of around 7 kN, showed a gradual decline in load, and had a prolonged failure before a complete rupture, which showed that the non-exposed ones had better ductility. Freeze-thaw was not carried out for the CFRP + resin reinforced specimen due to some internal machine issues, and the frequency and dynamic modulus did not decrease over the time taken to reach 300 cycles for the former specimens that were tested.

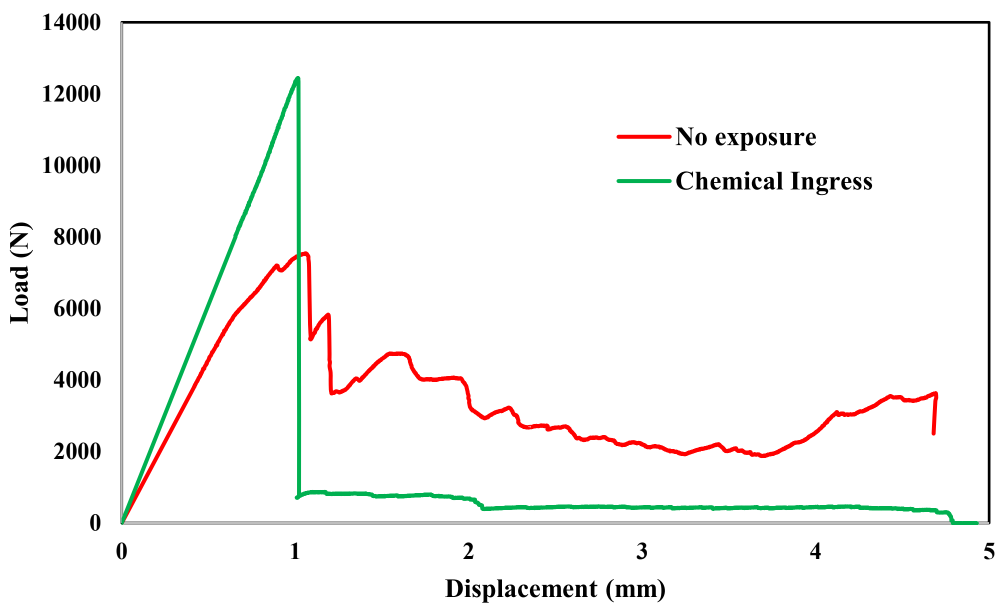

Figure 39: GFRP+ Resin reinforced specimen testing after chemical ingress and no exposure

Load-displacement behavior of the non-reinforced specimens exhibits a brittle nature with very low deformation capacity. The chemically ingressed specimen experienced the highest load of ~ 23 to 24 kN before abrupt and complete rupture. The unexposed specimen registered a moderate peak load of ~ 11 kN, followed by abrupt failure characteristic of brittle material without reinforcement. The freeze-thaw specimen exhibited the lowest capacity of ~ 10 kN, indicating that repeated freeze-thaw cracking triggered cracks that reduced the bond strength and ductility. All the non-reinforced specimens had a sudden brittle failure. Figure 40 describes the crack propagation of the freeze-thawed non-reinforced specimen, and Figure 41 shows load vs displacement for non-reinforced specimens.

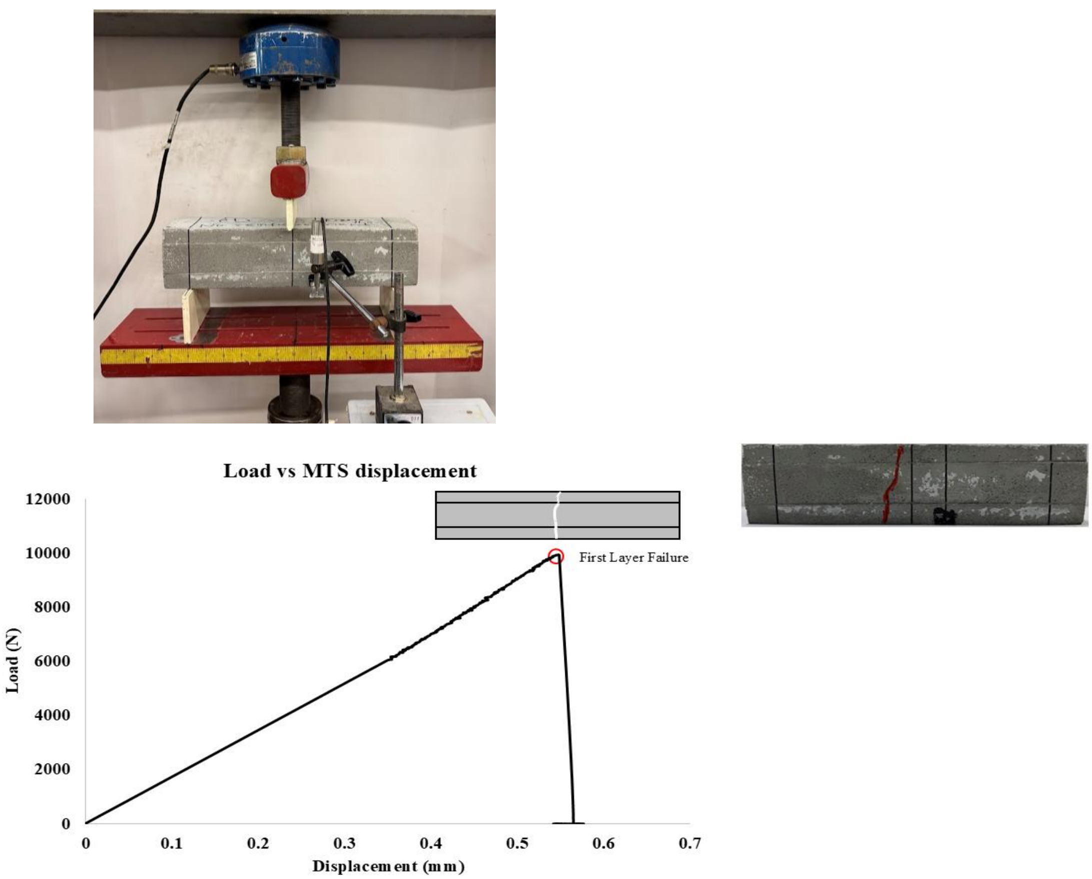

Figure 40: Load vs Displacement of non-reinforced specimen after freeze-thaw exposure

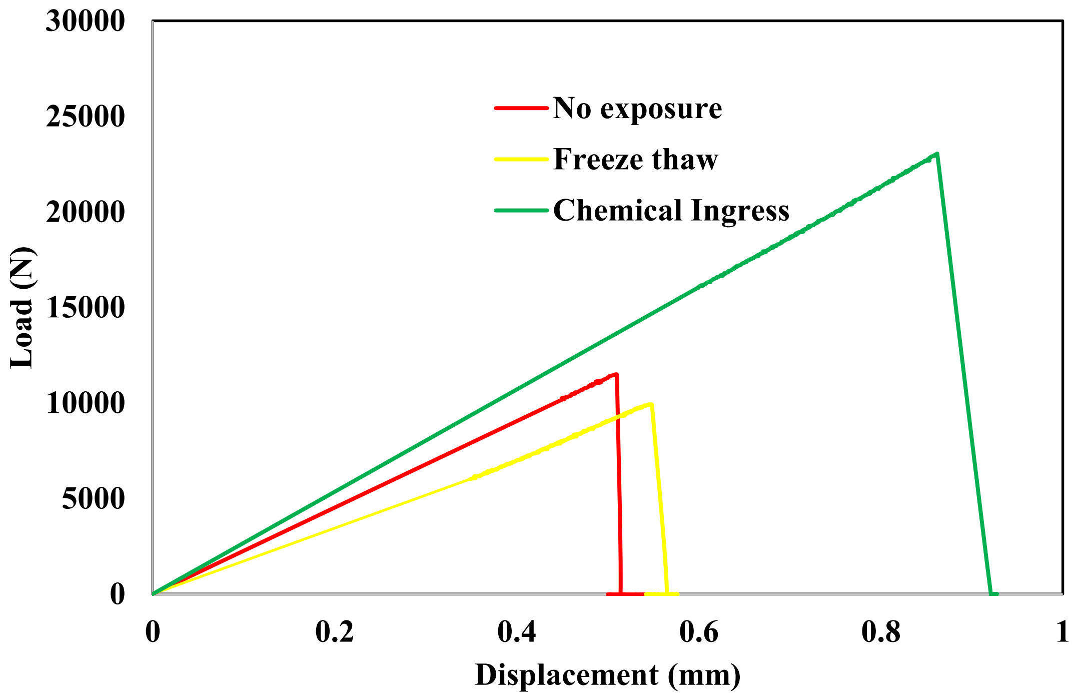

Figure 41: Non-reinforced specimen testing after freeze-thaw, chemical ingress, and no exposure

6 Concrete 3D Printer – Installation and Setup

A concrete 3D printer named Scara Elite Roadrunner 4M was acquired from 3D Potter located in Palm City, FL. The printer is combined with the roadrunner track, which adds another axis of control, allowing flexibility in creations for full-size structures and walls. The printer consists of Scara Elite V2 and Roadrunner rail system, pump arm with hose adaptor, gearbox cover, allen key set, lithium grease syringe, floor screws, Z rail adjuster, and power supply equipment. The printer is capable of printing at high speeds; however, speed is relative when it comes to cementitious 3D printing. Many factors determine the speeds, like nozzle size, layer height, and achieving good adhesion on the interlayer plays a major role in how the print moves forward. Figure 42 shows the 3D Printer's configuration.

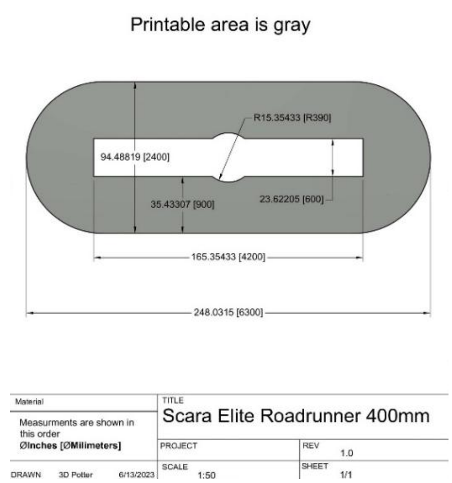

a) b)

Figure 42: (a) Scara Elite Roadrunner 4M with extruder pump, (b) Plan view of printer with dimensions

6.1 Assembly

The assembly of Scara Elite Roadrunner 4M has four different sub-sections listed below.

6.1.1 Unpacking and inventory

All the components were laid out (frame, robot arm, electronics, extruder, and hoses). The manufacturer's packing list was matched with the components received, noting any missing/damaged items before proceeding, which is depicted in Figure 43.

a) b)

Figure 43: (a) and (b) Inventory of Scara Elite Roadrunner 4M

6.1.2 Fixing the X-rail and base frame

The base should be bolted first as per guidelines, but the manufacturer suggested assembling everything first, and if necessary, it would be very easy to shift it. The rail system was fixed on the ground using a spirit level and a square to ensure the base is flat, which can be seen in Figure 44.

Figure 44: Fixing of X-rail in ground

6.1.3 Fixing the probes and assembling the Z-rail

The X, Y, Z, and U probes are fixed in place, which are the sensors provided by manufacturers for each direction for getting commands, understanding the movement in each direction, and are very sensitive to damage. All the probes and arms are properly synchronized. The probes help to stop the automated system and robotic arm from halting its movement from that point and work as a dead end for that arm and also help the robotic arm and rails to know their exact position for itself, so that a set of instructions from the user is better understood by the machine. This can be seen in Figure 45.

a) b) c)

Figure 45: (a) Fixing of robotic arm, (b) Fixing of Z-rail, (c) Fixing of probe sensors

6.1.4 Installation of extruder pump and rotor-stator

Extruder pump from IMER group named IMER Might Small 50, which pumps out to the hose that is attached to the rotor-stator when concrete is poured into the hopper. The mixture contained in the hopper is sucked by the rotor-stator pumping system and pushed into the hose until it reaches the opposite end of the hose. The pump's speed is controlled through the exclusive IMER A1 inverter, adapting the machine to different needs. Also, the pump is equipped with a diagnostic display, which signals any anomalies during use and related resolution methods. The images are in Figure 46.

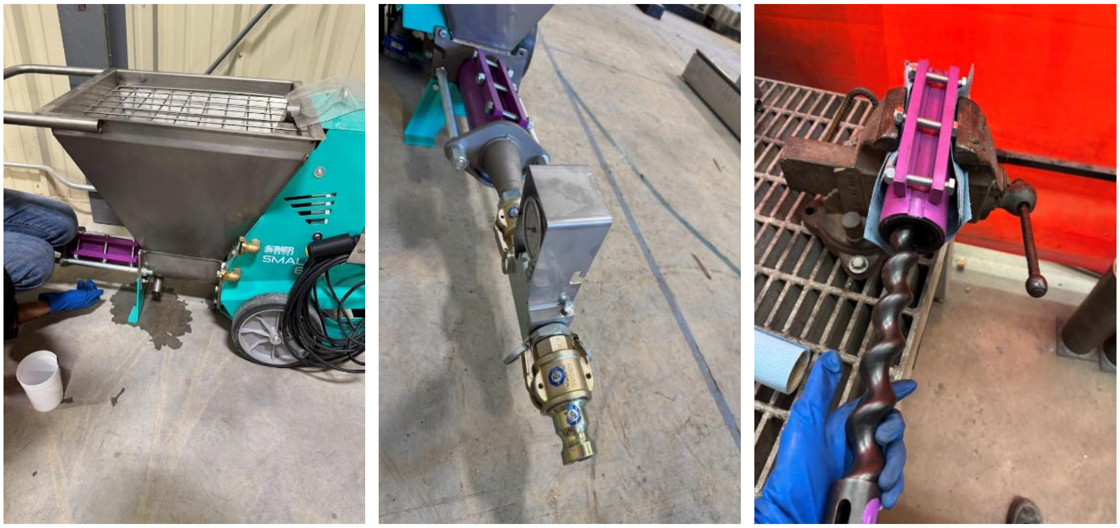

a) b) c)

Figure 46:(a) IMER Mighty Small 50 pump, (b) Extruder and hose attachment, (c) Rotor-stator attachment

6.2 3D Modeling Software

SketchUp 3D software was used to develop the 3D model. 4-in x4-in x15-in beams were designed and modeled using SketchUp 3D. Web web-based free version was used for most of the designs, including the specimens. The files created in SketchUp 3D shall be exported to. stl format for the slicing software.

6.3 Slicing Software

Simplify3D was used. It is a commercial slicing software (licensed) used to prepare 3D models for printing. It converts 3D models (STL, OBJ, 3MF) into G-code (Geometric code) instructions for the printer. Simplify3D is well known for the high customizability of slicing parameters and multiple process settings like extruder, layers, and infill patterns. The slicing is very accurate and supports easy generation of sliced prints and editing.

Also, it is compatible with hundreds of printers worldwide. The file is subjected to the "Prepare to print" option exclusively for Simplify3D. The sliced model can be seen in the figure below. "Orange" is the infill pattern, whereas "blue" is the perimeter layer. Figures 47, 48 and 49 show the Simplify3D software interfaces.

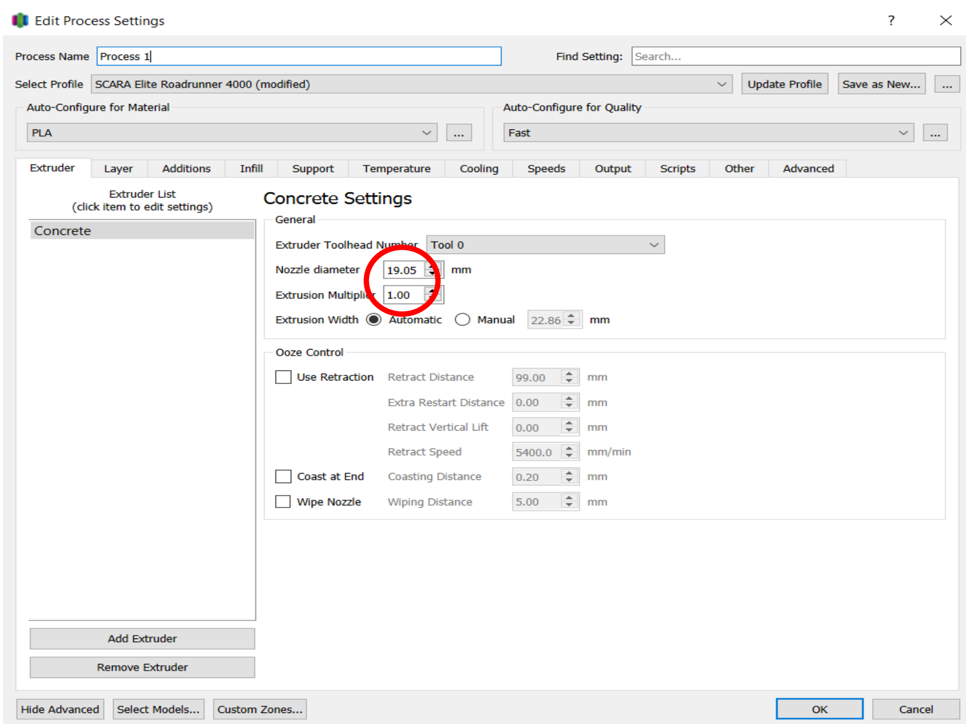

Figure 47: Nozzle diameter and extruder configuration

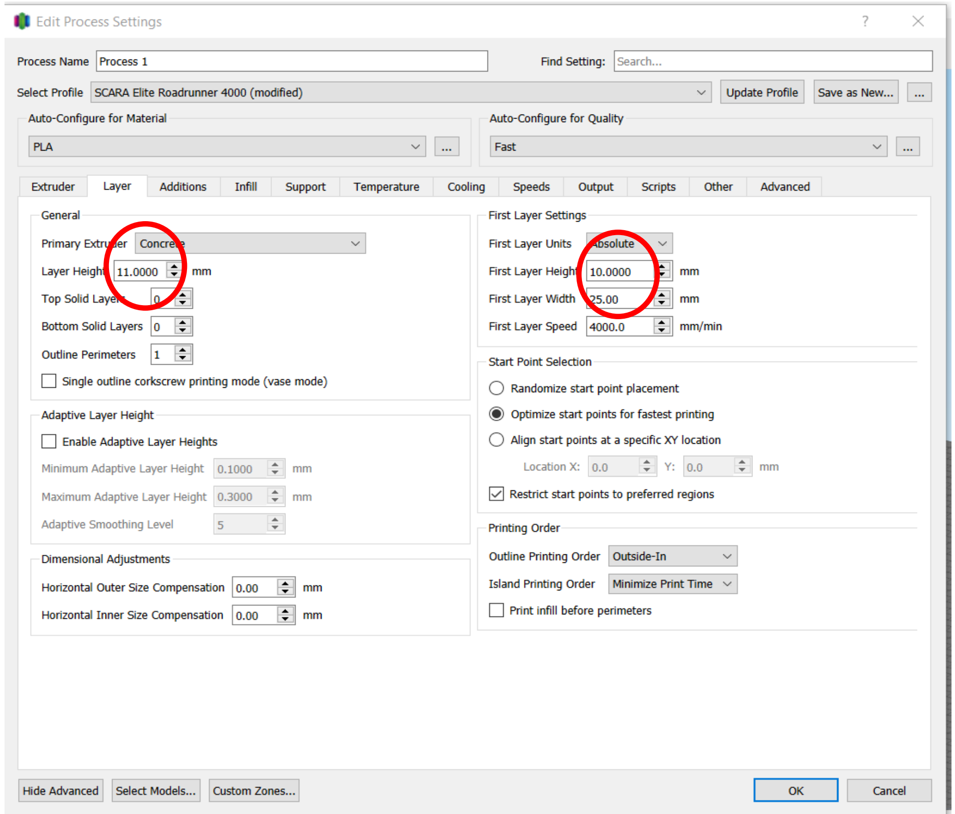

Figure 48: First layer height and layer height configuration

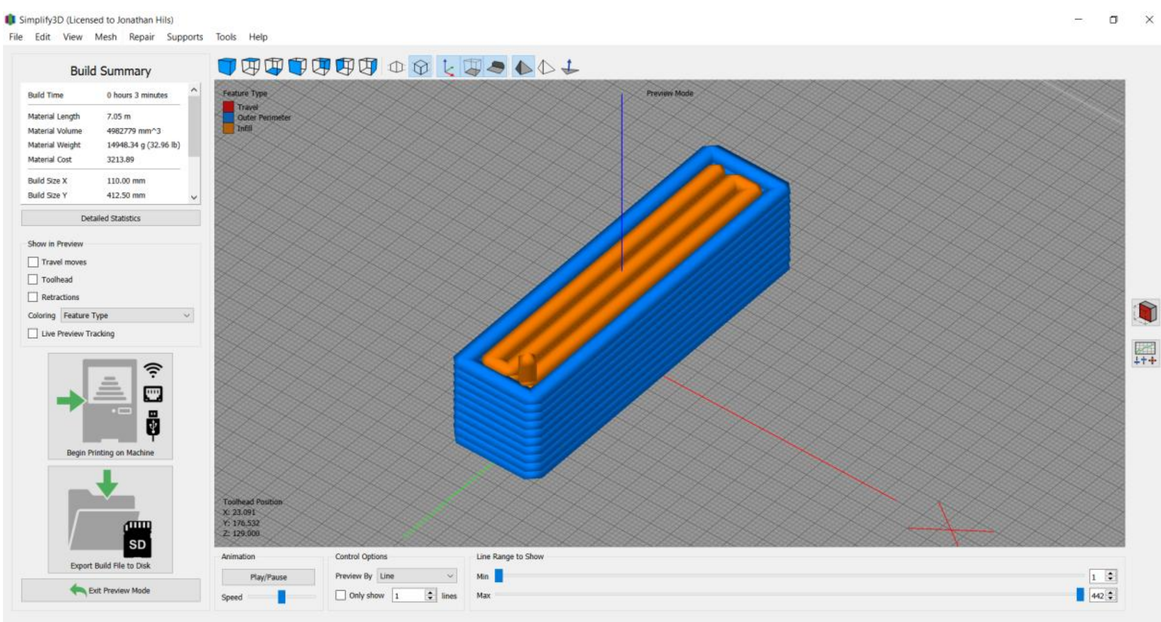

Figure 49: Sliced 4-in x 4-in x 15-in beam

6.4 G-codes

G-code stands for geometric code. It is the numerical control (NC) language used to tell machines (like 3D printers) what movements to take and where. Each line of G-code is a series of instructions like move in Z-axis, home all, set speed to 25, extrude material, etc. The most common command is G28, which is a homing code set by the manufacturer, where G stands for geometry. A series of G-code commands is given to the 3D printer, and a successful print is achieved. Figure 50 shows the 3D Potter's printing interface.

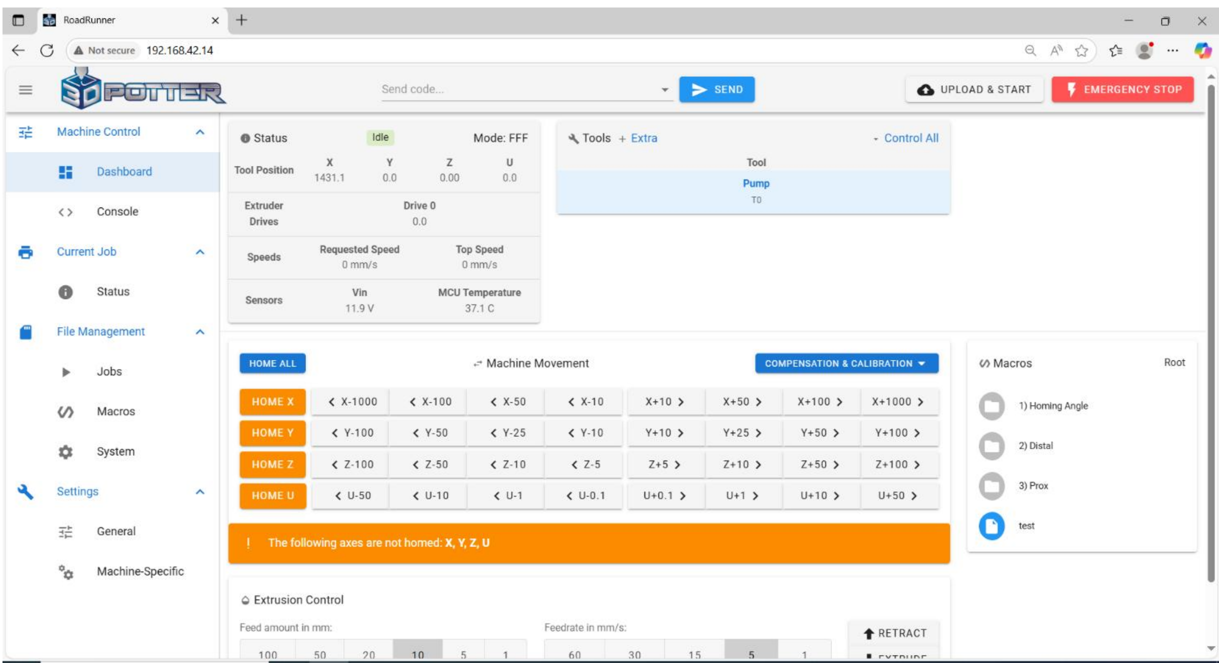

Figure 50: Dashboard of Scara Elite Roadrunner software

6.5 Printing specimens

Once the 3D printer is set up and operation checks are complete, the proposed mix design was used to fabricate the beam specimens of the same size of 4-in x 4-in x 15-in as the 3D printed beam specimens. The Scara Elite Roadrunner 4M concrete 3D Printer shall be used with an extrusion pump, which is necessary equipment for extruding the concrete out of the nozzle. The 3D printer is shown in Figure 42. The step-by-step printing involves first mixing the concrete and making sure the concrete does not set quickly. The set time obtained was 140 minutes which was already checked during the concrete mix selection process. Then, power on the 3D printer and the pump, making sure that the print is already programmed to the 3D printer. Then, turn the pump on and wait for the 3D printer to print the designed pattern.

In 3D printing, the stacking sequence is critical, as each lower layer must possess sufficient strength to support the layers deposited above it, continuing progressively throughout the entire build. Figure 51 depicts the proper layer stacking configuration once a new print is completed.

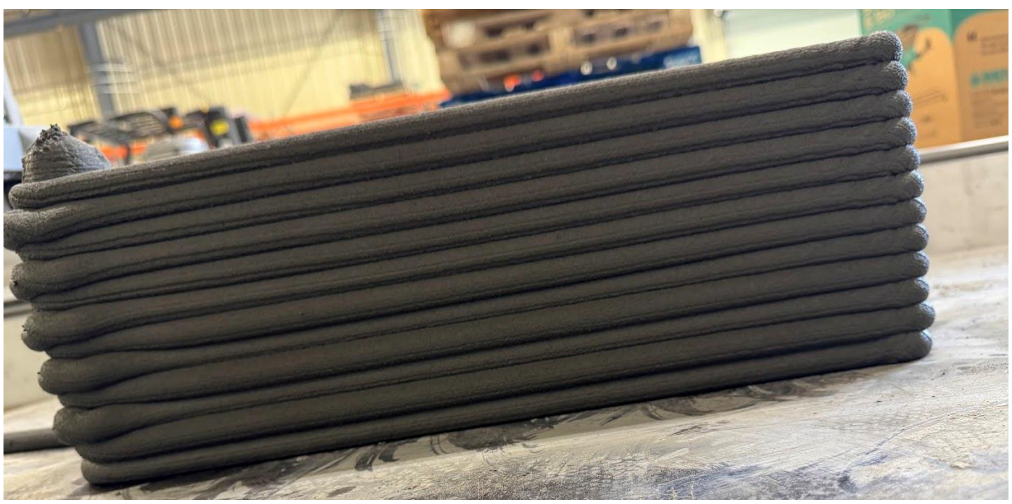

Figure 51: Stacking sequence of 3D Printed concrete

7 Phase B: 3D Printed Specimens

7.1 Mix design

The mix design for 3DPC plays a vital role in assuring proper printability and, ability to gain proper tensile and overall structural performance. An ideal mix design should possess proper printability, possessing a rheological profile that allows smooth extrusion without segregation or clogging. Also, the printed mix should be able to retain the shape while providing a proper stacking sequence with a proper bond between the adjacent layers. The mix should be durable enough to restrain the ingress of chemicals through it. Chlorides, sulfates, and carbon dioxide are highly permeable compounds that tend to attack and ultimately deteriorate the mix. Also, the mix should be able to support the weight of the top layers. Incorporating additives like fibers and reinforcement can contribute to the ductility and tensile capacity. Mix should also be able to handle the freezing and thawing mechanisms. The mix is shown in Table 3 and particle size distribution curve can be seen in Figure 52.

Table 3: Components of mix design for Phase B

Material	Quantity
Cement	546 kg/m^3
Fly Ash	156 kg/m^3
Silica Fume	78 kg/m^3
Masonry Sand	1171 kg/m^3
Water	219 kg/m^3
High-range Water Reducer (HRWR)	8.2 kg/m^3

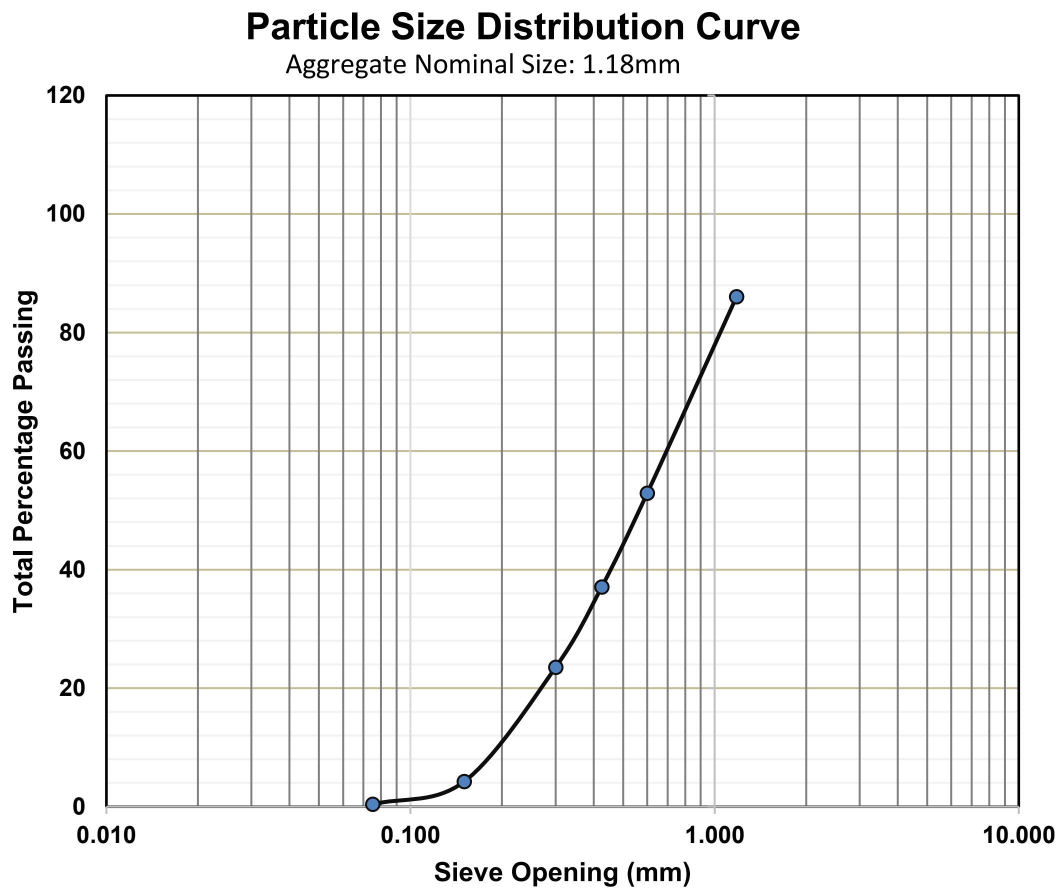

Figure 52: Particle size distribution curve for masonry sand

7.2 Non-reinforced

Non-reinforced 3D printed specimens are printed using Simplify3D model and g-code as mentioned. The instructions shall be given to the machine, and the nozzle height needs to be adjusted before printing to have a smooth and unbroken print. Mix should be good enough to hold the layers so that a proper stacking sequence can be achieved; for that 7.75-in flow should be necessary. This can be seen in Figure 53 and how the layer thickness and height achieved can be seen in Figure 54.

Figure 53: 3D printed non-reinforced specimens

Figure 54: 3D Printed non-reinforced layer thickness and height

7.3 Reinforced

Reinforced 3D printed specimens are printed using Simplify 3D model and g-code as mentioned. The instructions shall be given to the machine, and the nozzle height needs to be adjusted before printing to have a smooth and unbroken print. Mix should be good enough to hold the layers so that a proper stacking sequence can be achieved; for that 7.75-in flow is necessary.

7.3.1 Steel reinforcement

3D printed steel reinforced beams were fabricated in a step-by-step manner. The first two layers of 3D printed concrete were stacked on top of each other, which was approximately. the same layer thickness as the manually fabricated ones. The first 1-in layer was printed with concrete and had no compaction. The printing was paused for reinforcement placement. Then, manually, the steel fabric was placed, and again the printing process was resumed. The printing process continued until the second layer of reinforcement was placed at 1-in from the top surface. And finally, the top clean surface was achieved. The printer stops by itself when printing is done. The steel mesh and specimen can be seen in Figure 55.

a) b)

Figure 55: (a) 3D Printed beam with steel reinforcement, (b) Fabric for steel reinforcement

7.3.2 GFRP

3D printed GFRP reinforced beams were fabricated in a step-by-step manner. The first two layers of 3D printed concrete were stacked on top of each other, which was approximately. the same layer thickness as the manually fabricated ones. The first 1-in layer was printed with concrete and had no compaction. The printing was paused for reinforcement placement. Then, manually, the GFRP fabric was placed, and again the printing process was resumed. The printing process continued until the second layer of reinforcement was placed around 1-in from the top surface. And finally, the top clean surface was achieved. The printer stops by itself when printing is done. The mesh and specimen can be seen in Figure 56.

a) b)

Figure 56: (a) Placement of fabric in 3D Printed specimens and printing specimens, (b) Checking the level for printed specimens

7.3.3 CFRP

3D printed CFRP reinforced beams were fabricated in a step-by-step manner. The first two layers of 3D printed concrete were stacked on top of each other, which was approximately. the same layer thickness as the manually fabricated ones. The first 1-in layer was printed with concrete and had no compaction. The printing was paused for reinforcement placement. Then, manually, the CFRP fabric was placed, and again the printing process was resumed. The printing process continued until the second layer of reinforcement was placed around 1-in from the top surface. And finally, the top clean surface was achieved. The printer stops by itself when printing is done.

The mesh and specimen can be seen in Figure 57.

a) b)

Figure 57: (a) Placement of fabric in 3D Printed specimens, (b) Checking the level for printed specimens

7.4 Reinforcement with resin

7.4.1 GFRP

3D printed GFRP + resin reinforced beams were fabricated in a step-by-step manner. The first two layers of 3D printed concrete were stacked on top of each other, which was approximately. the same layer thickness as the manually fabricated ones. The first 1-in layer was printed with concrete and had no compaction. The printing was paused for reinforcement placement. The resin+hardener mix was created and applied through a roller as shown in the figure below. That wet GFRP fabric was then manually placed, and again the printing process was resumed. The printing process continued until the second layer of reinforcement was placed around 1-in from the top surface. And finally, the top clean surface was achieved. The printer stops by itself when printing is done. The mesh and specimen can be seen in Figure 58.

a) b)

Figure 58: (a) 3D printing on wet GFRP fabric, (b) Wet GFRP fabric

7.4.2 CFRP

3D printed CFRP + resin reinforced beams were fabricated in a step-by-step manner. The first two layers of 3D printed concrete were stacked on top of each other, which was approximately. the same layer thickness as the manually fabricated ones. The first 1-in layer was printed with concrete and had no compaction. The printing was paused for reinforcement placement. The resin+hardener mix was created and applied through a roller as shown in the figure below. The wet CFRP fabric was then manually placed, and again the printing process was resumed. The printing process continued until the second layer of reinforcement was placed around 1-in from the top surface. And finally, the top clean surface was achieved. The printer stops by itself when printing is done. The mesh and specimen can be seen in Figure 59.

a) b)

Figure 59: (a) 3D printing on wet CFRP fabric, (b) Wet CFRP fabric

7.5 3D Printing Problems

3D printing concrete, however, being a new and innovative technology that involves creating objects using a printer, has its own challenges that make the job a bit tricky at the beginning. The numerous problems that were encountered with both the printer and the rotor-stator-equipped extruder pump are described in the following sections.

7.5.1 Fine aggregates

The fine aggregates that were used for Phase A mix had a nominal aggregate size of 2.36mm, which was used for the extruder pump to extrude out of the printer's hose. Unfortunately, the machine and the hose were clogged, and heating with fumes from the end of the hose was detected. Addressing the problem to the manufacturer (3D Potter), who mentioned prior to mixing that the 2.36mm should have worked fine with the pump and the printer; however, this was not the case. This problem was solved by using a modified mix design mentioned in Phase B. Also, this was the sole reason for the change in fine aggregate for the 3D printed mix compared to the manually fabricated specimens.

7.5.2 Temperature

Temperature played a vital role in the process of printing. At first, when the printing started, temperatures were low; hence, the amount of high-range water reducer was good enough to make the mix workable, and the set time that was achieved was 140 minutes. However, during an extremely hot summer, the mix's workability was altered and became stiff very quickly. Hence, the amount of HRWR was altered by 5% to get close to the ideal parameters necessary for the printing process. Figure 60 shows the effect of temperature on the mix.

a) b)

Figure 60: (a) Flow achieved in winter with same amount of HRWR, (b) Flow achieved in summer with same amount of HRWR

7.5.3 Rotor and Stator configuration

The rotor and stator are the main shaft of the engine for the extruder pump. The mix fed to the pump shall be pushed to the hose using these components. Rotor and stator are very sensitive to the type of mix, fine aggregate's gradation, workability of the mix, and the volume of the mix fed to the extruder pump. Multiple trial and error were performed for the type of mix so that the rotor stator would not produce any heat. Once heated, it would be very tough to get the stator out as it would be locked, having the concrete mix inside, with the high temperature causing the concrete to set. The only solution was to create an ideal mix so that the rotor and stator system keep running, given that enough mix should be in the pump so that a good-quality print can be achieved. Figure 61 shows the rotor stator configuration.

Figure 61: Rotor (pink) and Stator (black spiral rod)

7.6 Flexural Tests

When all the 3D printed specimens are cured and aged in respective chemical ingress chamber, the specimens are taken out and placed under a 250 kN MTS 810 hydraulic frame using LVDT sensors at a displacement of 1mm/min on mid span, which shall provide the necessary deflection data with load following ASTM C580 and ASTM C78. The setup is shown in Figure 62. The load is applied until the specimen’s failure. Failure surfaces shall be thoroughly studied.

Figure 62: Flexural test setup

7.7 Testing and Results

OU's signature logo was 3D printed in the Fears laboratory, shown in Figure 63. The same Phase B mix design was used.

Figure 63: 3D printed University of Oklahoma's logo

7.7.1 Deterioration Mechanisms

7.7.1.1 Chemical Ingress

Like manual fabrication, a chemical ingress chamber is created with water and 6% NaCl solution. Sulfuric acid is added regularly to maintain a pH less than or equal to 2. After that, the 28-day cured beam specimens are placed in the chamber, and ingress is measured at 30-day intervals for 60 days and ultimately for 90 days. Beam specimens are progressively deteriorated due to the chemical that is being ingressed inside the specimens through the interface. Similarly, some specimens had an orange texture, which is a sign that, due to the chemical ingress, the specimens are getting weaker. This can be observed in Figure 64.

Figure 64: Chemical ingress chamber with 6% NaCl and pH < 2

7.7.1.2 Steel reinforcement

Steel reinforced specimens have seen a greater deterioration over the period of 60 and 90 days than the ones that are unexposed. Unexposed ones had no discoloration and deterioration over time, whereas for the 3D printed ones, when steel in concrete begins to corrode, it forms iron oxides (rust) and iron hydroxides, which often appear orange, reddish-brown, or yellowish, which is because of chloride and sulfate exposure. This can be clearly seen in Figure 65.

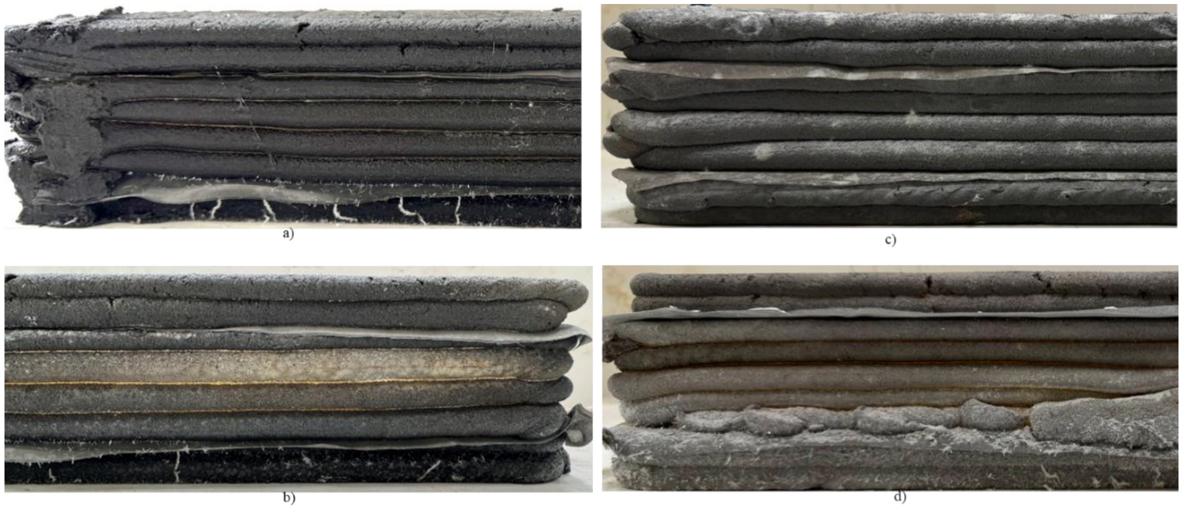

Figure 65: Steel (a) 60 days unexposed, (b) 60 days chemical exposure, (c) 90 days unexposed, (d) 90 days exposed

7.7.1.3 GFRP

GFRP reinforced specimens also saw some significant deterioration over the course of 60 and 90 days. The unexposed specimen was uniform in color and texture for both 60 and 90 days. No visible discoloration was observed along the printed interfaces. The GFRP mesh also remained intact and clean, showing no sign of chemical deterioration. This indicates a good bond and durability under normal curing conditions. For the exposed ones, a brownish/orange color was visible along the layers – a sign of chemical reaction due to exposure for 60 days. The deterioration was similar to the 90-day-exposed specimens. The discoloration indicates migration of soluble salts through the layer interface. This can be seen in Figure 66.

Figure 66: GFRP (a) 60 days unexposed, (b) 60 days chemical exposure, (c) 90 days unexposed, (d) 90 days exposed

7.7.1.4 GFRP + Resin

GFRP, with resin-reinforced specimens, also saw some significant deterioration over the time of 60 and 90 days. The unexposed specimen was uniform in color and texture. No visible discoloration was observed along the printed interfaces. The GFRP mesh that was dipped into resin + hardener mix also remained intact and clean, showing no sign of chemical deterioration. This indicates a good bond and durability under normal curing conditions. For the exposed ones, a brownish/orange color was easily visible along the layers – a sign of a huge chemical reaction due to exposure for 60 and 90 days. The discoloration indicates migration of soluble salts through the layer interface. This can be seen in Figure 67.

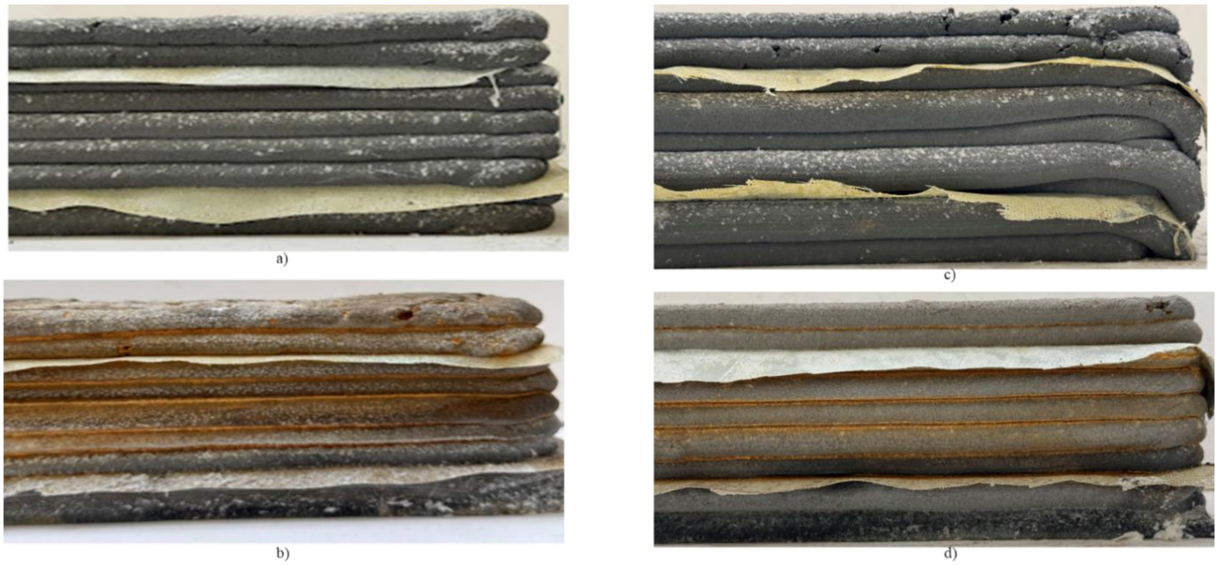

Figure 67: GFRP+Resin (a) 60 days unexposed, (b) 60 days chemical exposure, (c) 90 days unexposed, (d) 90 days exposed

7.7.1.5 CFRP

CFRP reinforced specimens also saw some significant deterioration over the time of 60 and 90 days. The unexposed specimen was uniform in color and texture. No visible discoloration was observed along the printed interfaces. The GFRP mesh also remained intact and clean, showing no sign of chemical deterioration. This indicates a good bond and durability under normal curing conditions. For the exposed ones, a brownish/orange color was visible along the layers – a sign of chemical reaction due to exposure for 60 and 90 days. The discoloration indicates migration of soluble salts through the layer interface. Moreover, significant salt deposition can be seen in the specimens exposed for 90 days. This can be seen in Figure 68.

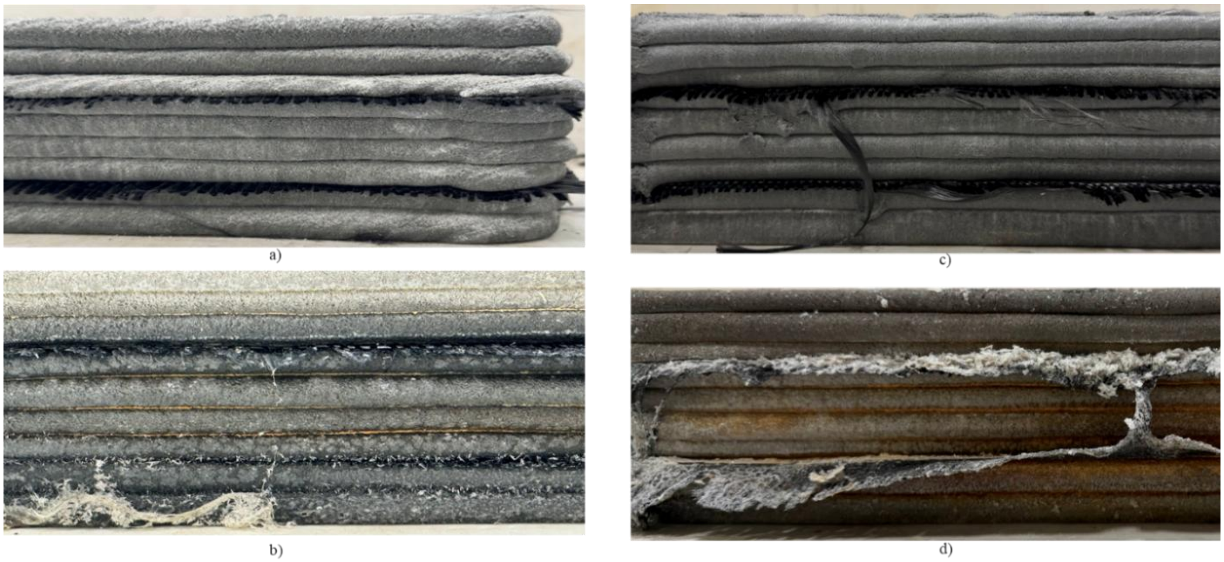

Figure 68: CFRP (a) 60 days unexposed, (b) 60 days chemical exposure, (c) 90 days unexposed, (d) 90 days exposed

7.7.1.6 CFRP + Resin

CFRP, with resin-reinforced specimens, saw some significant deterioration over the time of 60 and 90 days. The unexposed specimen was uniform in color and texture. No visible discoloration was observed along the printed interfaces. The CFRP mesh with resin + hardener also remained intact and clean, showing no sign of chemical deterioration. This indicates a good bond and durability under normal curing conditions. For the exposed ones, a brownish/orange color was clearly visible along the layers – a sign of chemical reaction due to exposure for 60 days. The brown texture was significant on the 90-day-exposed specimen than in the 60-day-exposed one. The discoloration indicates migration of soluble salts through the layer interface. This can be seen in Figure 69.

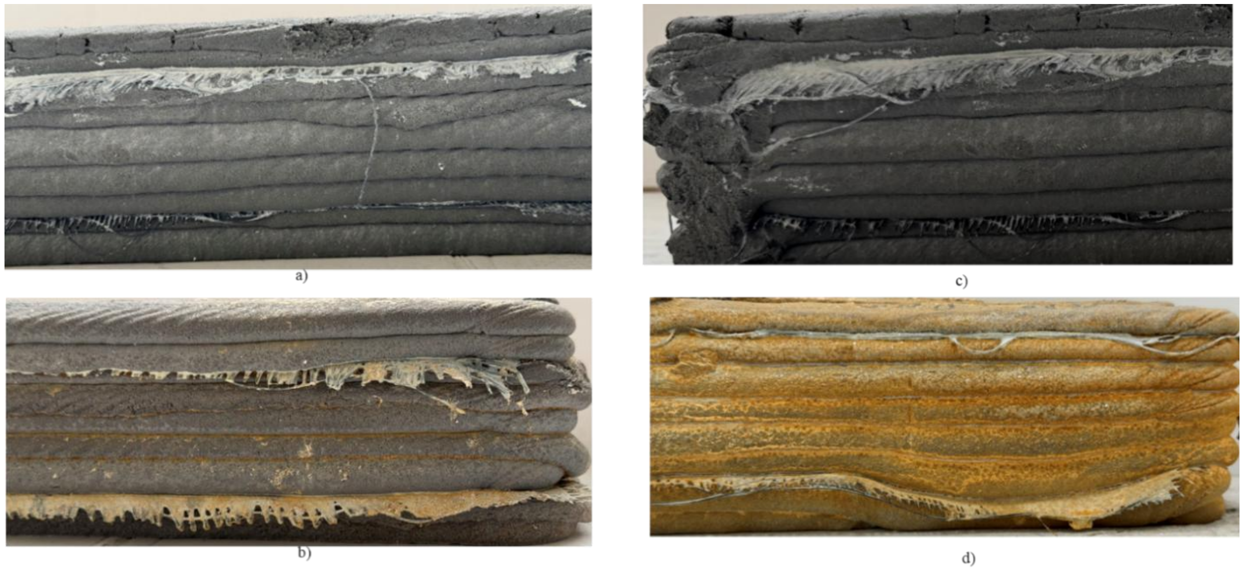

Figure 69: CFRP + Resin (a) 60 days unexposed, (b) 60 days chemical exposure, (c) 90 days unexposed, (d) 90 days exposed

7.7.1.7 No reinforcement

Non-reinforced 3D printed specimens were also impacted when exposed for 60 and 90 days in the chemical chamber. The discoloration and deterioration were visible and prominent. The discoloration was also very surprising for the non-reinforced ones, but a possible explanation would be; all the specimens were under the same tub for exposure, hence, the color might have transferred, and also the reaction between the mix and the acid solution in the presence of salt can also form by-products which might have produced orangy/yellowish texture to the non-reinforced beam. There was no visible deterioration for the unexposed ones, and they were mostly pristine, whereas for the exposed ones, a brownish/orange color was clearly visible along the layers – a sign of chemical reaction due to exposure for 60 and 90 days. The discoloration indicates migration of soluble salts through the layer interface. This can be seen in Figure 70.

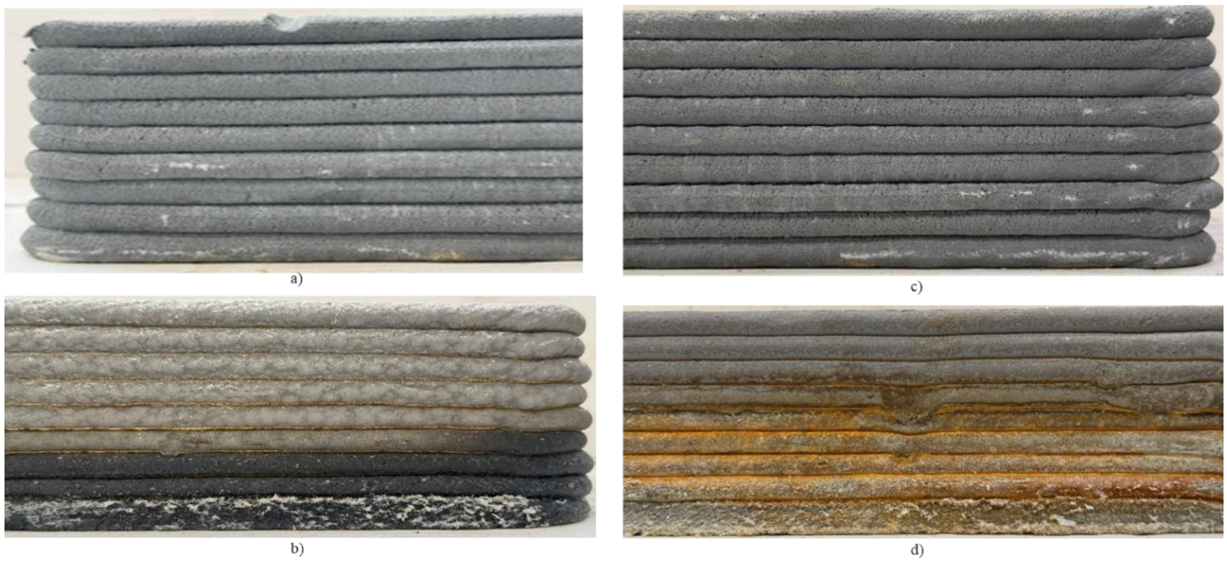

Figure 70: Non-reinforced (a) 60 days unexposed, (b) 60 days chemical exposure, (c) 90 days unexposed, (d) 90 days exposed

7.7.2 Freeze-thaw

Freeze-thaw testing for 3D printed specimens was not conducted primarily due to the ever-increasing upward trend for the manually fabricated specimens. The mix design for the 3D printed specimens has a very comparable compressive strength to the manually fabricated ones, though not the same. The freeze-thaw chamber freeze phase occurs at -18 °C (0 °F), and the thawing occurs at 4 °C (40 °F). The test is supposed to stop when the relative dynamic modulus of elasticity at given cycle ‘n’ is obtained when the frequency at ‘n’ cycles is 60-70% of its initial value, but it never occurred to any of the specimens. Hence, the freeze-thaw process was not performed for the 3D printed ones. Additionally, the freeze-thaw machine had some technical difficulties, and due to the space and time limitations, the freeze-thaw was discarded for the 3DPC.

7.7.3 Load vs Displacement

Load vs displacement from flexural tests were plotted for each of the 3D printed beam specimens for the chemically exposed and unexposed specimens. Each of the chemically exposed specimens had a progressive failure mechanism rather than catastrophic collapse failure, except for the non-reinforced specimens.

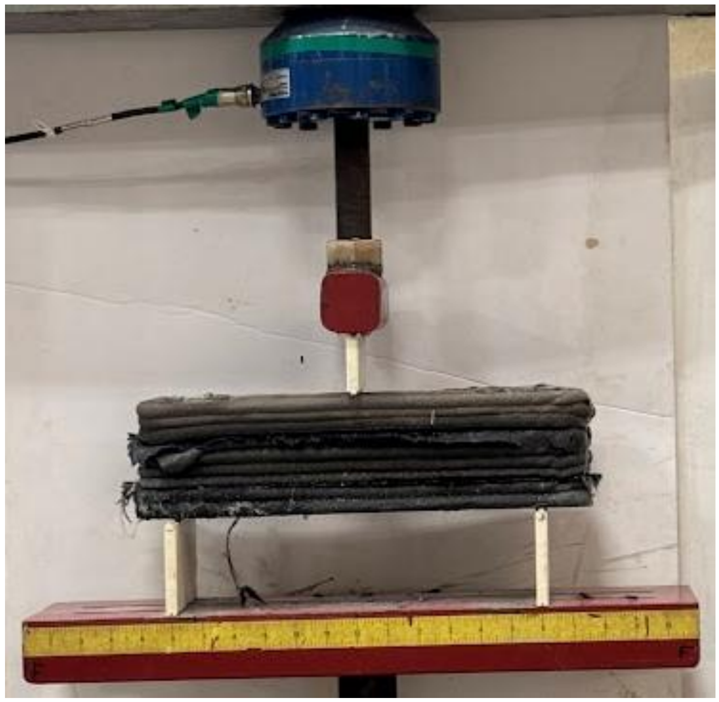

Figure 71: Experimental setup for 3D Printed CFRP specimen under MTS frame

The experimental setup for CFRP reinforced beams flexural testing can be seen in Figure 71. Failure patterns can be seen for each of the CFRP reinforced specimens in Figure 72. There was no complete rupture or brittle failure for any of the CFRP-reinforced specimens; however, the ones with resin had a significant area under the curve before failure.

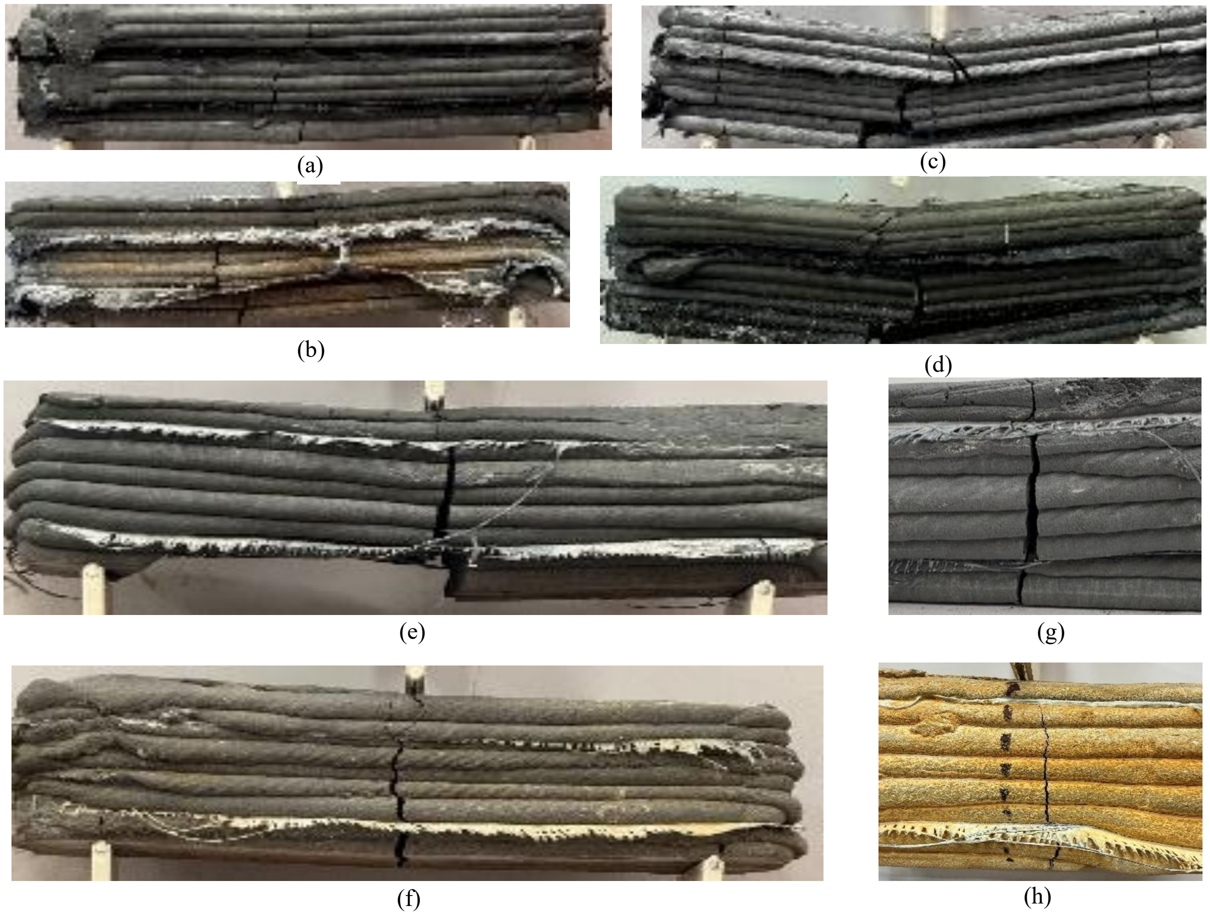

Figure 72: Failure images for (i) CFRP-Reinforced specimens (a) 60 days unexposed, (b) 60 days exposed (c)90 days unexposed, (b) 90 days exposed

(ii) CFRP+Resin -Reinforced specimens (e) 60 days unexposed, (f) 60 days exposed, (g) 90 days unexposed, (h) 90 days exposed

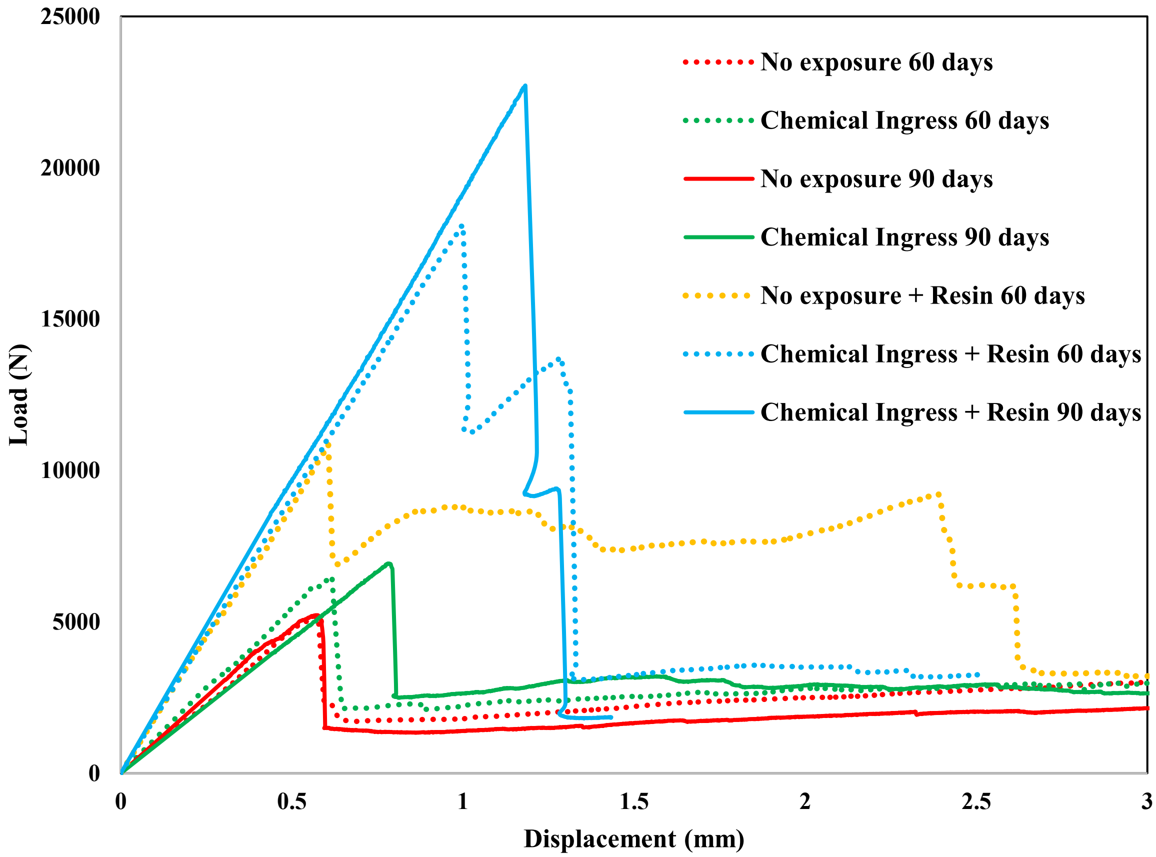

Figure 73: Load vs Displacement of CFRP-reinforced 3D printed specimens

The load vs displacement of CFRP reinforced beams was heavily dependent on the environmental conditions. The highest maximum load (~22.5 kN) was associated with beam samples after 90 days, i.e., Chemical Ingress + Resin. Beam samples 60 days with Chemical Ingress + Resin also had a high peak load (~18 kN), as did the non-exposed beam samples with 60 days (~10.7 kN). Specimens that did not have resin on them were significantly weaker than specimens with resin. For instance, Chemical Ingress - 90 days reached a maximum load of ~6.8 kN, and Chemical Ingress 60 days reached ~6.4 kN. Non-exposed beams, however, were significantly lower, with values ranging from ~5.0 kN to 5.2 kN. The ranking of stiffness determined a hierarchy with a stiffness ranking order of CI+R_90 > CI+R_60 > NE+R_60 > CI_90

> CI_60 > NE_90 > NE_60, demonstrating the impact of resin treatment and long-duration exposure. Notably higher stiffness did not necessarily transfer to improved post-peak ductility, given the differences in toughness behaviors; NE+R_60 was highest, followed by CI_90, NE_90, CI_60, NE_60, CI+R_90, and finally CI+R_60. Unfortunately, there was a problem with the beam NE+R_90; hence, the data was discarded. Overall, strength increased by approximately 5% from 60 to 90 days for non-resin specimens, while with resin, chemically ingressed beams exhibited a more substantial 20% increase, highlighting the significant enhancement in strength provided by resin in aggressive environments. The plot can be seen in

Figure *73*.

Figure 74: Experimental setup for 3D Printed Steel specimen under MTS frame

The experimental setup for steel-reinforced beams' flexural testing can be seen in Figure 74.

Failure patterns can be seen for each of the steel-reinforced specimens in Figure *75*. There was no complete rupture, but there was a prolonged failure for all the steel-reinforced specimens.

Figure 75: Failure images for Steel-Reinforced specimens (a) 60 days unexposed, (b) 60 days exposed, (c)90 days unexposed, (b) 90 days exposed

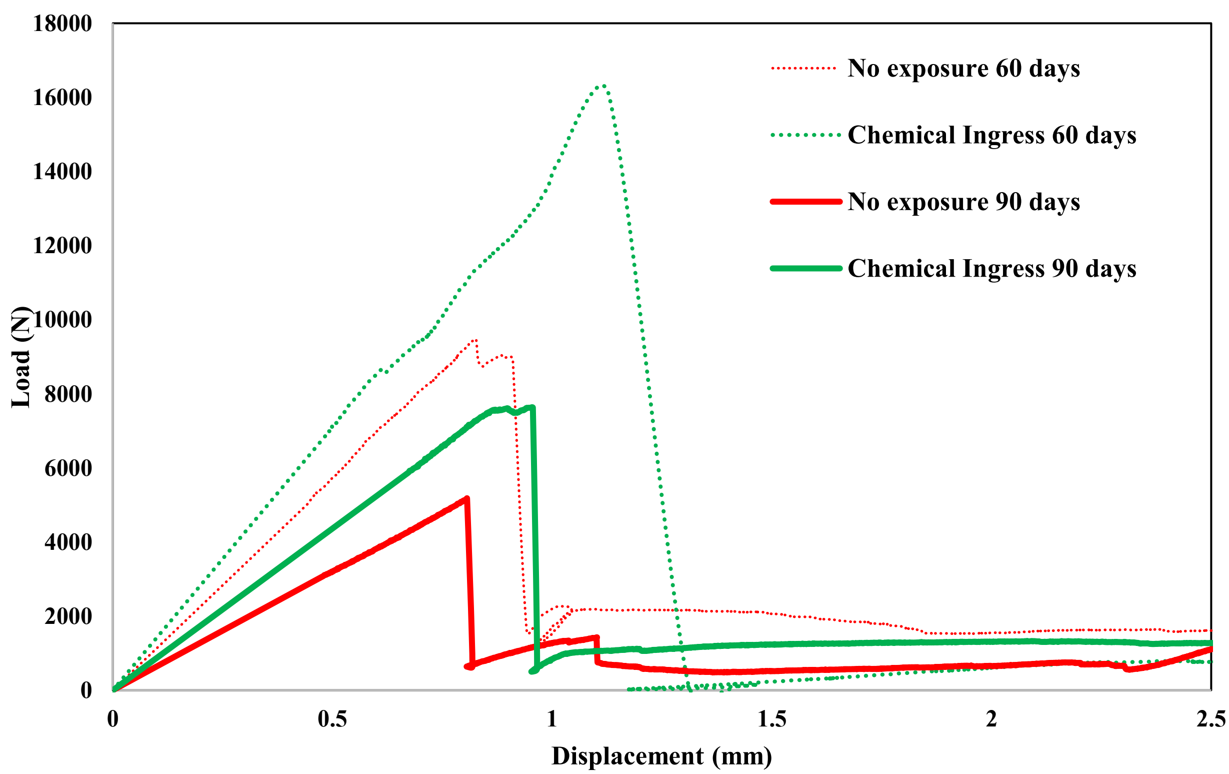

Figure 76: Load vs Displacement of Steel-reinforced 3D printed specimens

Steel-reinforced specimens have demonstrated evident degradation with time, as indicated by prolonged exposure. The specimens that have been chemically exposed for 60 days developed the highest peak loads of approximately 16 kN, while the non-exposed members after 60 days had peak loads around 9.5 kN. The chemically exposed specimens developed at 90 days at a moderate peak load of approximately 7.6 kN, and the non-exposed specimens developed at the lowest at around 5.2 kN, showing the least resilient and most brittle response, as evidenced by their low capacities and high failure stiffness. The stiffness rankings developed from 60 to 90 days are as follows: CI_60 > NE_60 > CI_90 > NE_90, and the toughness ranking is shown as: NE_60 > CI_90 > CI_60 > NE_90, showing that the early-age non-exposed members of the specimens retained more energy after peak-load failure than the exposed members did. The reason for the great loss of stiffness from 60-90 days of exposure can be attributed to corrosion of the reinforcement steel of the exposed specimens, which lessened composite action. Over the 60 to 90-day exposure period, the amount of peak load that was lost due to deterioration of the composite specimens was approximately 50%, indicating severe structural degradation with extended exposure. It is interesting to note that the 60-day chemically exposed specimens were still hydrating in immersion condition at 90 days, which accounts for the increase in stiffness as compared to the non-exposed specimens. The plot can be seen in Figure 76.

Figure 77: Experimental setup for 3D Printed GFRP specimen under MTS frame

The experimental setup for GFRP reinforced beams flexural testing can be seen in Figure 77. Failure patterns can be seen for each of the GFRP reinforced specimens in Figure 78. There was brittle failure for any of the GFRP-reinforced specimens.

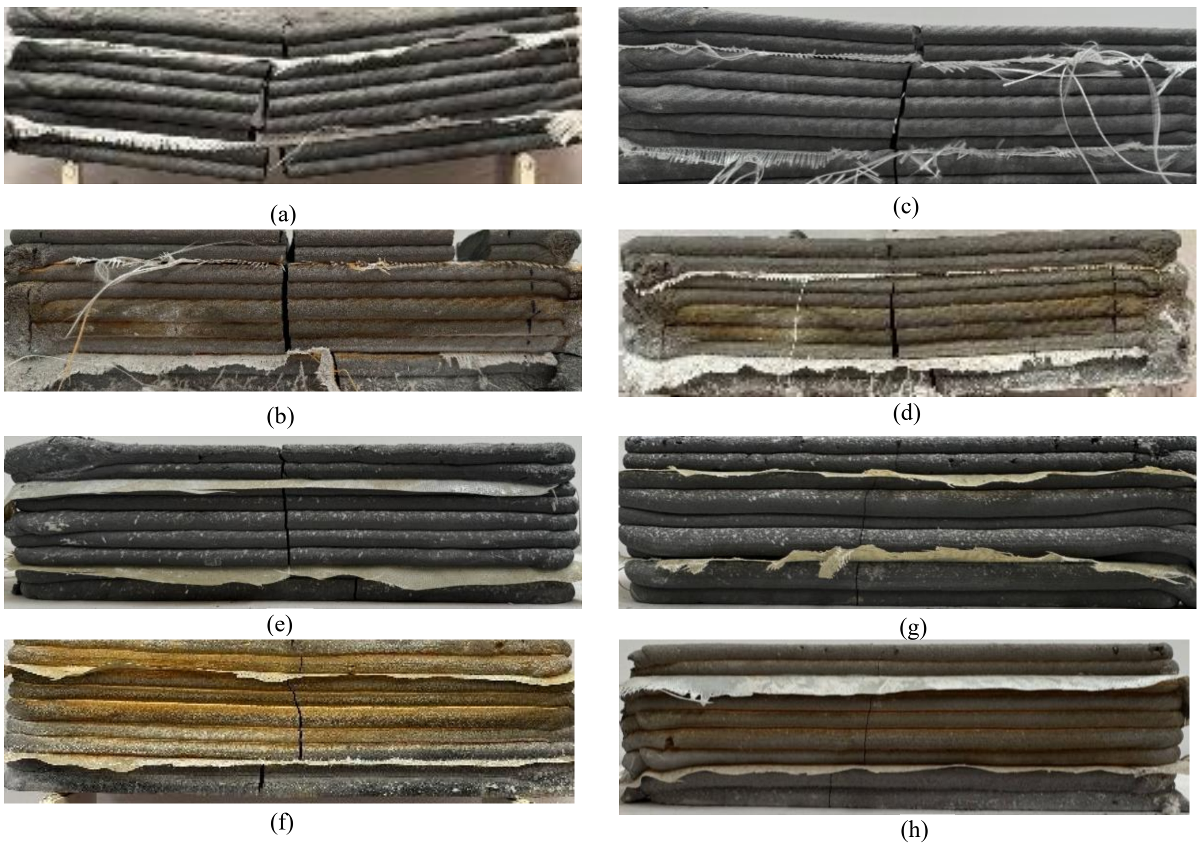

Figure 78: Failure images for (i) GFRP-Reinforced specimens (a) 60 days unexposed, (b) 60 days exposed (c)90 days unexposed, (b) 90 days exposed

(ii) GFRP+Resin -Reinforced specimens (e) 60 days unexposed, (f) 60 days exposed, (g) 90 days unexposed, (h) 90 days exposed

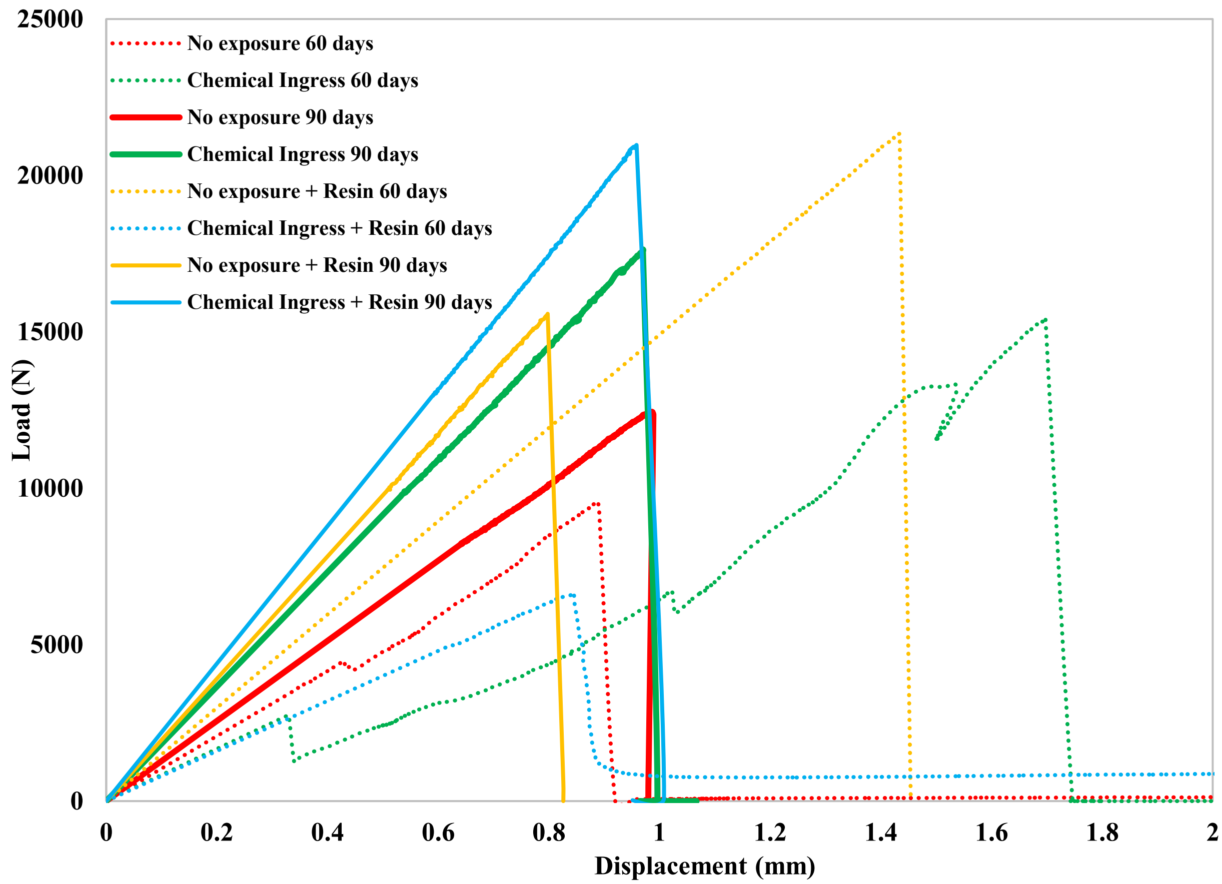

Figure 79: Load vs Displacement of GFRP-reinforced 3D printed specimens

In terms of the beams reinforced with GFRP, the highest level of peak load (~20.8 kN) was displayed by the specimens that were chemically exposed plus the resin for 90 days and very closely followed by the unexposed specimens plus the resin for 60 days (~21.2 kN), indicating the resin was a contributor to the enhanced bonding in this case at early ages. The specimens that were chemically exposed for 90 days performed at a moderate level of capacity (~17.5 kN); the non-exposed specimens with resin that were exposed for 90 days and the chemically exposed specimens with resin that were exposed for 60 days performed equally (~15.5 kN and ~15.3 kN, respectively). However, the non-exposed specimens at both 90 and 60 days had the lowest recorded peak loads (~12.3 kN and ~9.6 kN, respectively), while the chemically exposed specimens with resin that were exposed for 60 days had the most failed peak loads (~6.6 kN). The stiffness ranking was CI+R_90 > NE+R_60 > CI_90 > NE+R_90 > CI_60 > NE_90 > NE_60 > CI+R_60, whereas the toughness ranking was NE+R_60 > CI_90 > NE_90 > NE_90 > CI_60 > NE_60 > CI+R_90 > CI+R_60, indicating that the resin used on the specimens exposed for 60 days was a major contributing factor to enhancing energy absorption. An approximate 12% average increase in peak strength was identified between the 60 and 90 days on exposed specimens: most likely attributed to continuing hydration of the specimens as a result of chemical exposure. Predominantly, the failure mode of the specimens was brittle and was influenced by having limited ductility following the peak. The plot can be seen in Figure 79.

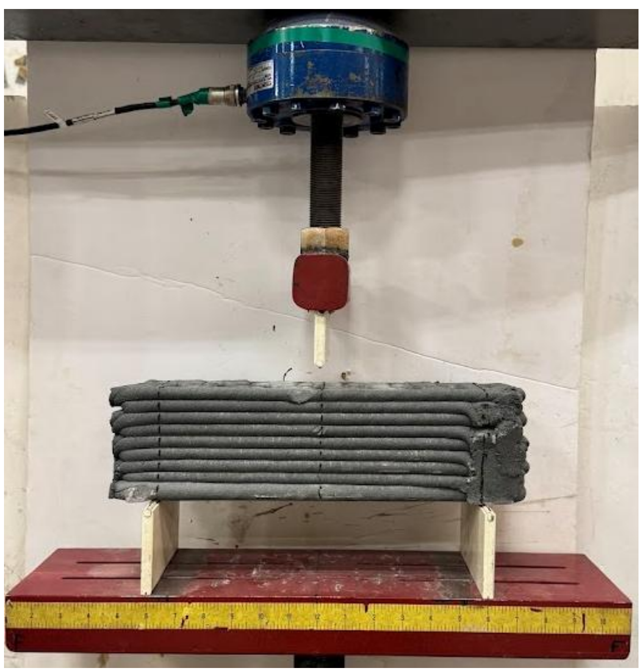

Figure 80: Experimental setup for 3D Printed non-reinforced specimen under MTS frame

The experimental setup for non-reinforced beams' flexural testing can be seen in Figure 80. Failure patterns can be seen for each of the CFRP reinforced specimens in Figure 83. There was a complete rupture or brittle failure for any of the non-reinforced specimens.

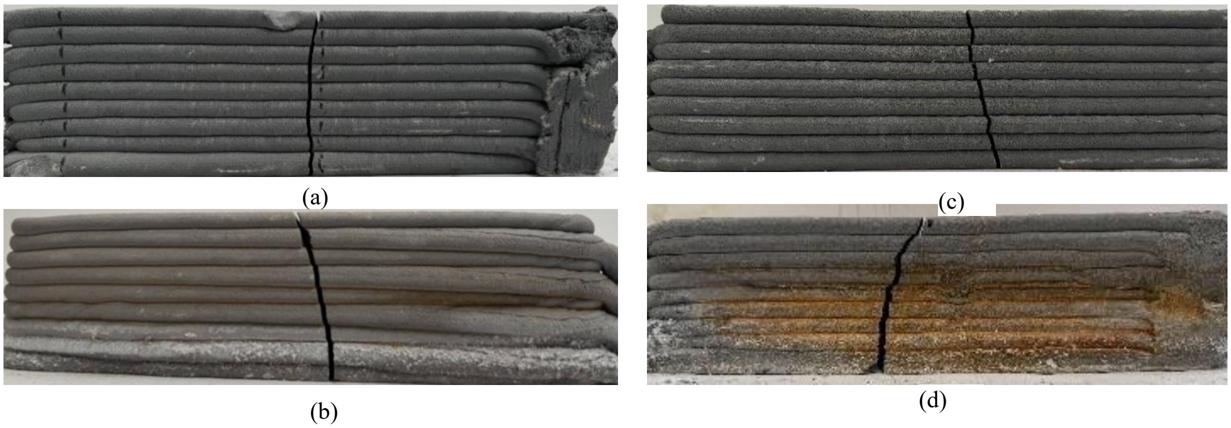

Figure 81: Failure images for non-reinforced specimens (a) 60 days unexposed, (b) 60 days exposed, (c) 90 days unexposed, (b) 90 days exposed

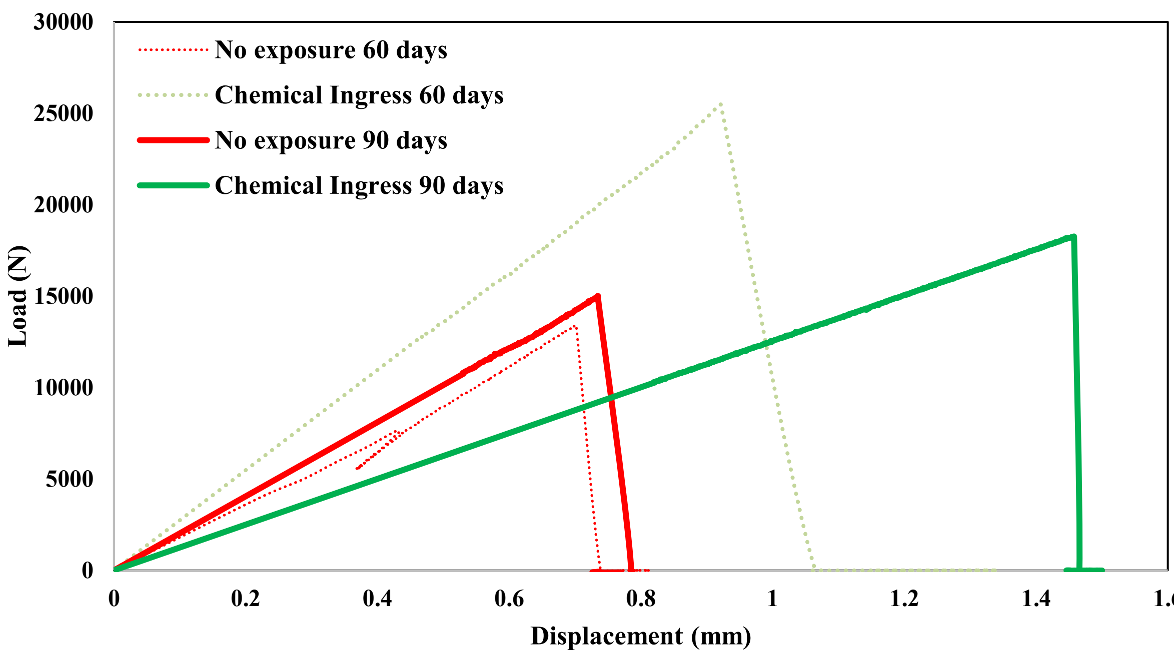

Figure 82: Load vs Displacement of non-reinforced 3D printed specimens

The non-reinforced 3D printed beam specimens showed a brittle failure when subjected to three-point loading under the MTS frame. The non-exposed (NE) ones for both 60 and 90 had a lower peak load, both approximately 15 kN, whereas the highest one is the Chemical Ingress (CI) specimen, which achieved a peak of 25 kN, and the 90-day ones achieved a peak load of 17.5 kN. This suggests that the chemical exposure increased the strength of the concrete beam before cracking, which could be from pore filling, surface hardening, or secondary mineral or chemical formation during the hydration process. Non-exposed specimens show lower strength, possibly due to a more porous matrix or the lack of surface densification effects. Since no reinforcement is present in all specimens, the specimens lost almost all load-carrying capacity immediately. The plot can be seen in Figure 82.

8 Microscopic analysis

The failed specimens from flexural tests were analyzed using light microscopy. The Keyence VHX-7000 ultramicroscope at the Samuel Roberts Noble Microscopy Laboratory on the University of Oklahoma campus was utilized to investigate the failure modes of flexural specimens. Each type of reinforcement used shall be different, so failure mode and crack propagation may be different due to varying conditions. Hence, microscopic validation of the failure interfaces focused on understanding reinforcement behavior, bond between binder and reinforcement, and failure modes with exposed and un-protected vs exposed and protected interlayers were performed on all tested specimens.

8.1 Deteriorations due to exposure

The exposed specimens showed visible rusty-orange deposits upon inspection; therefore, sections of these specimens – particularly around the interface – were further examined. Based on the investigation and proof of salty-type crystals forming on Figure 83. Investigation and some relevant literature revealed that ettringite, its crystal type and texture, which was present in the sample, was completely based on inspection, giving the rusty orange texture to the crystals. Ettringite **(**$Ca_6Al_2(SO_4)_3(OH)_{12}\cdot 26H_2O$**)** is formed during the hydration process of the cement and used for the initial strength of concrete; however, its delayed formation causes surface roughness and microcracking, which works the opposite of the aid that it initially provides the concrete [53].

Moreover, after 60 days of exposure, significant deterioration can be observed in Figure 84, where CFRP reinforcement is investigated, which had CFRP strands that are debonded from the exposure, visible on the left side of the microscopic image. The outer resin coating has peeled or been eroded in sections, likely due to acidic and chemical-like chloride ions, which degraded the epoxy matrix that bonds the carbon fibers together. However, the chemical exposure did not completely weaken the fiber bundle, but it had reduced the interfacial adhesion between the fiber and resin, which can be seen getting engulfed with a foggy white layer all over the surface.

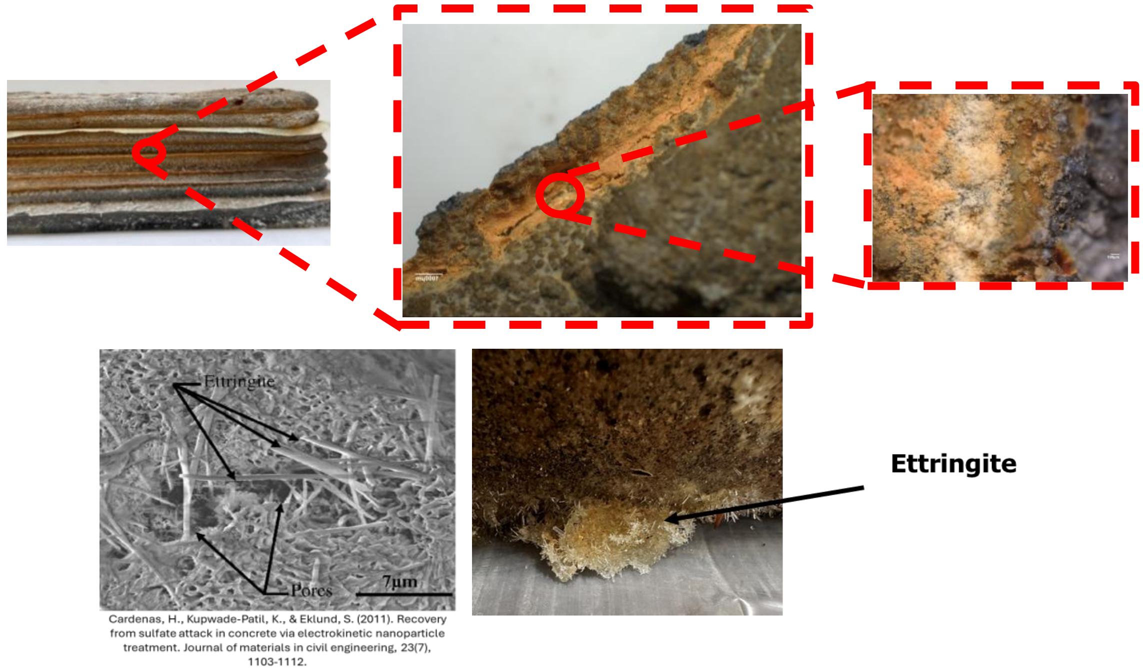

Figure 83: Microscopic investigation of 60 days exposed GFRP+Resin specimen and the presence of ettringite

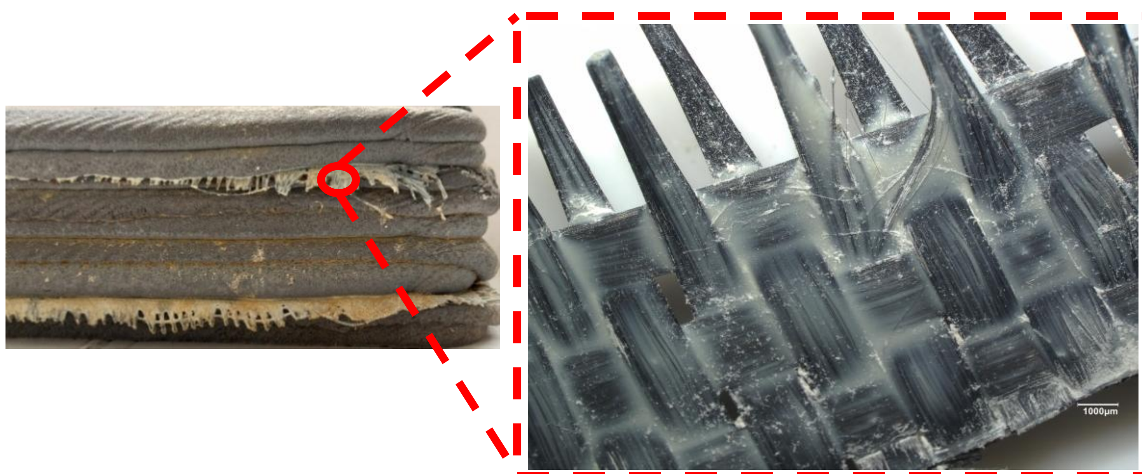

Figure 84: Microscopic investigation of 60 days exposed CFRP+Resin specimen focusing on reinforcement deterioration

The GFRP fabric shown in Figure 85 shows visible cracks and deterioration with significant discoloration, indicating chemical attack on the polymer matrix that binds the glass fibers. The yellow-brownish surface tone provides information on the by-products that are formed after exposure to the acid-salt mixture. The fiber bundle weave appears softened or partially dissolved, exposing the glass strands. Regarding the crack formation, the cracks were 30 to 35 µm wide, propagating both along and across fiber directions. These cracks were most likely formed due to mechanical shrinkage as the matrix degraded. The cracks suggested loss of interfacial cohesion due to chemical exposure, which accelerated along the fiber paths, deepening the cracks.

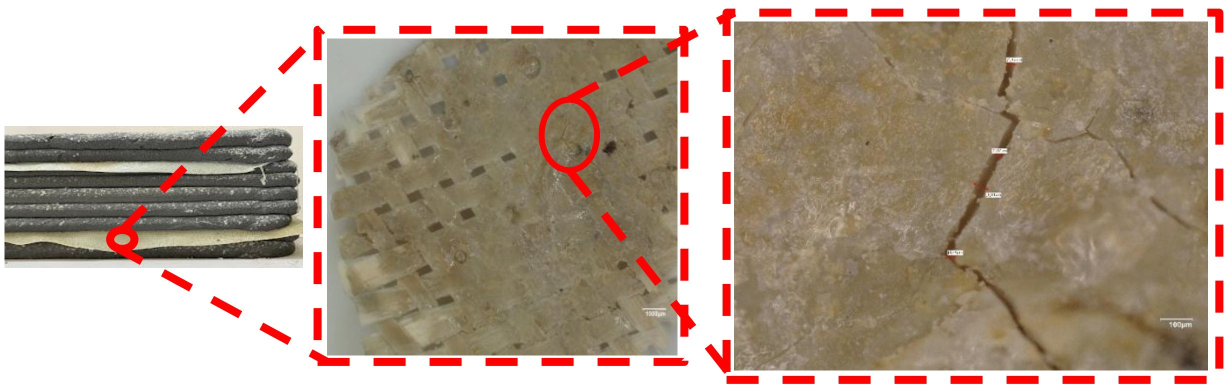

Figure 85: Microscopic investigation of 60 days exposed GFRP+Resin specimen focusing on reinforcement deterioration

The layered structure looks smooth and has well-bonded interfaces between the layers. This indicates that there are no significant delamination, voids, or segregation zones, which implies that the printing was good and proper interlayer adhesion, and compaction was achieved. This also concludes that any cracks or degradation that could be seen in the specimen could be from the environmental degradation due to exposure conditions. Small white patches near the interface could be calcium hydroxide crystals or unreacted cement grains, typically unexposed in cementitious materials, and are not a sign of degradation. Figure 86 shows the unexposed and non-reinforced 3D printed specimen's layer investigated under the microscope.

Figure 86: Microscopic investigation of 60 days unexposed non-reinforced specimen focusing on the layer

The steel fabric was extremely corroded after 90 days of exposure. The specimen was investigated under the microscope, where the formation of iron oxide or hydroxide can be seen, known as rust, which corrodes and decreases the strength of the beam. This corrosion can be seen in Figure 87. Also, the salt crystals that were in the specimen penetrated through the interface and can be seen attached to the steel mesh.

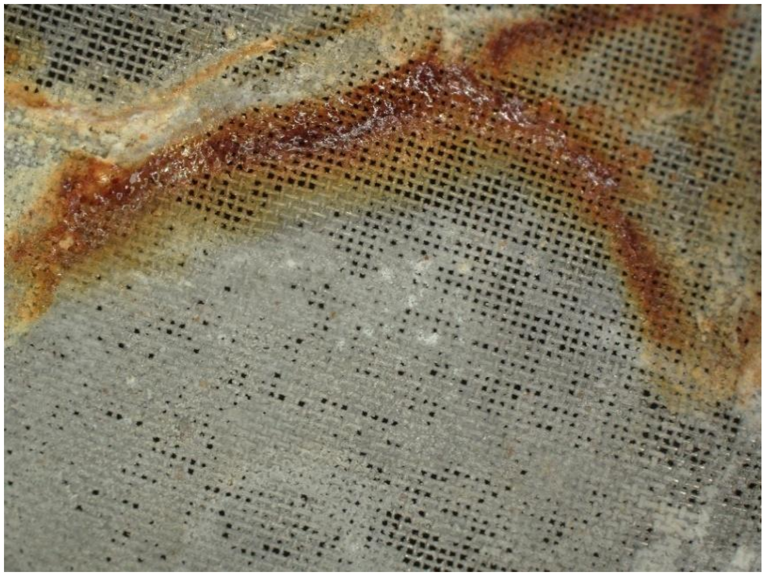

Figure 87: Microscopic investigation of steel fabric after 90 days of exposure

8.2 Post-failure deterioration

Specimens were tested after failure, where some were debonded, and some had cracks associated with it. 90-day-exposed specimens were investigated in the microscope, as seen in Figure 88. The CFRP reinforced specimen exposed for 90 days had concrete on the reinforcement surface incorporated between the layers, which is a clear sign of good bonding between the concrete and the reinforcement.

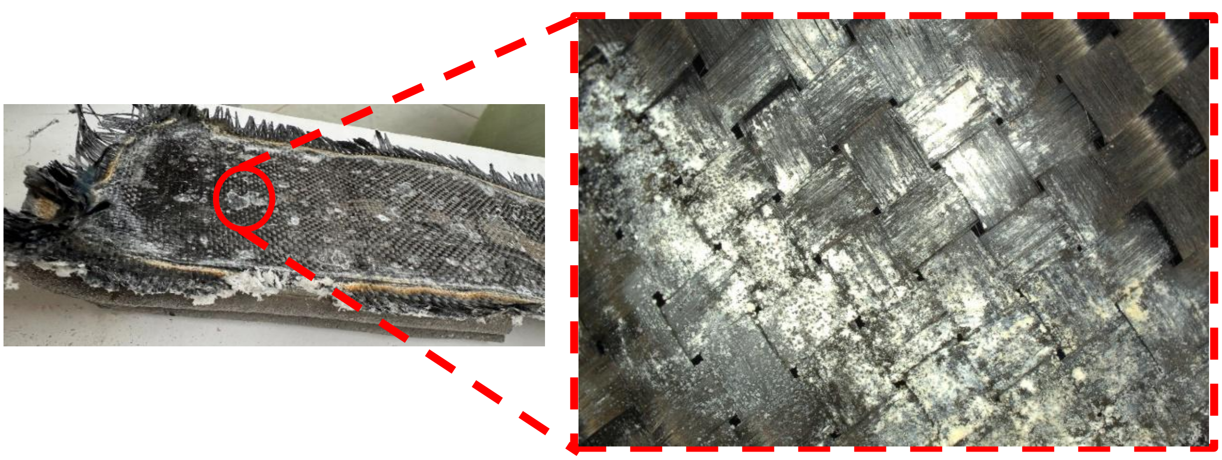

Figure 88: Microscopic investigation of 90 days exposed failed CFRP-reinforced specimen

The peeled-off CFRP specimen that was exposed for 90 days reveals clear evidence of interfacial debonding between the reinforcement layer and the concrete substrate. The specimen was peeled off manually, and the Keyence close-ups provide a better understanding of the failure mechanism. The upper enlarged section displays clean fiber surfaces and well-aligned woven fibers, whereas the lower one is the concrete surface. The woven fibers were measured in the same location in Keyence, investigating the bond between the reinforcement and concrete. The fibers in the concrete imply a good bond between them, which can be observed in Figure 89.

Observations were made at the edge of the GFRP-reinforced specimen that debonded after 90 days of exposure, since the overall bond was robust enough to prevent the fabric from being removed elsewhere. The interfacial area between the concrete and the fabric is depicted in the lower image, while the woven structure of the GFRP is highlighted in the upper-right image. A strong bond between the GFRP and the concrete substrate is shown by the difficulty in detaching the reinforcement. Also, some deterioration in the reinforcement was observed. This can be observed in Figure 90.

Figure 89: Microscopic investigation of a 90 days exposed failed CFRP reinforced specimen was conducted on the same spot

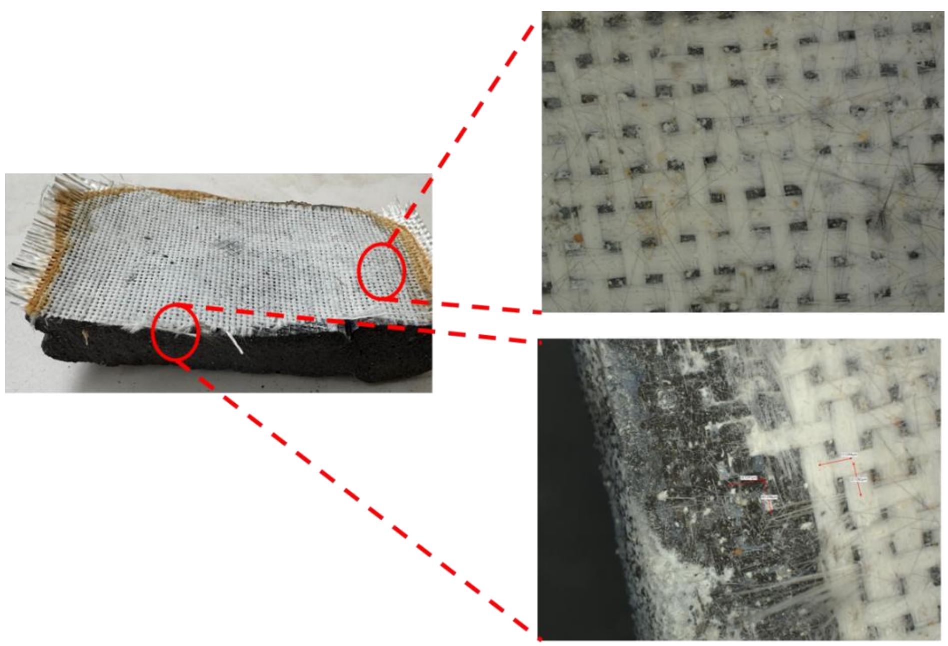

Figure 90: Microscopic investigation of a 90 days exposed failed GFRP reinforced specimen was conducted on the same spot

9 Discussions and Conclusions

The study investigated the durability performance of 3D printed and manually fabricated cementitious elements subjected to chemical ingress and non-exposed conditions. Mechanical testing was conducted for each specimen to determine peak load, post-peak behavior, and the flexural strength of each of the specimens. Steel reinforcement performed average in manual and was largely degraded by corrosion but improved a lot in the 3D printed ones when exposed to chemicals. For the manual specimens, steel in chemicals exposed lost 31% of its strength compared to non-exposed ones; however, it gained 41% of its strength when exposed to chemicals due to having better bonding in 3D printed ones.

3D printed non-reinforced specimens had a 28% reduction in their flexural resistance starting from 60 to 90 days of exposure; also, the steel-reinforced samples experienced a significant 50% reduction in their strength because of corrosion, which also showed the same trend. Talking about the FRP reinforced specimens, up to 60 days, the specimens (especially the resin-containing FRP systems) show improved flexural performance at 60 days, which suggests that curing is still active, additional C–S–H is forming, and the material is still in a strength-gain regime despite chemical exposure. At 90 days, a drop in strength that marks a behavioral shift. The 90-day results show a clear decline in strength compared to 60 days. Before 90 days, the C-S-H formed assisted the curing effects and that C-S-H assisted the specimen to dominate, which took a sharp turn after 90 days when degradation from chemical ingress began to dominate. This 90-day transition is the cutoff where the positive effects of curing are overtaken by the negative effects of chemical attack.

Microscopic observation, both the CFRP and GFRP fibers had significant damage due to chemical ingress. Slight erosion and interfacial debonding were observed, which explains the small oscillations in the plot. No significant and catastrophic damage due to cracking occurred for CFRP, proving that CFRP effectively resisted chemical degradation. Also, the peeling investigation proved that the bond between the concrete and the reinforcement was very good throughout the process, with an abundant amount of salt getting deposited in the reinforcement.

10 Recommendations for Future Work

Addressing the durability issues of 3D-printed specimens is covered under the 3D-Printed Solutions component of the project. These challenges arise because the printed elements contain layered interfaces through which chemicals can easily penetrate.

10.1 3D Printed Solutions

This study will provide solutions on how to minimize environmental deterioration affecting the 3DPC and investigate preventative measures. The major solutions that this study will investigate are listed in Figure 91 and [54, 55].

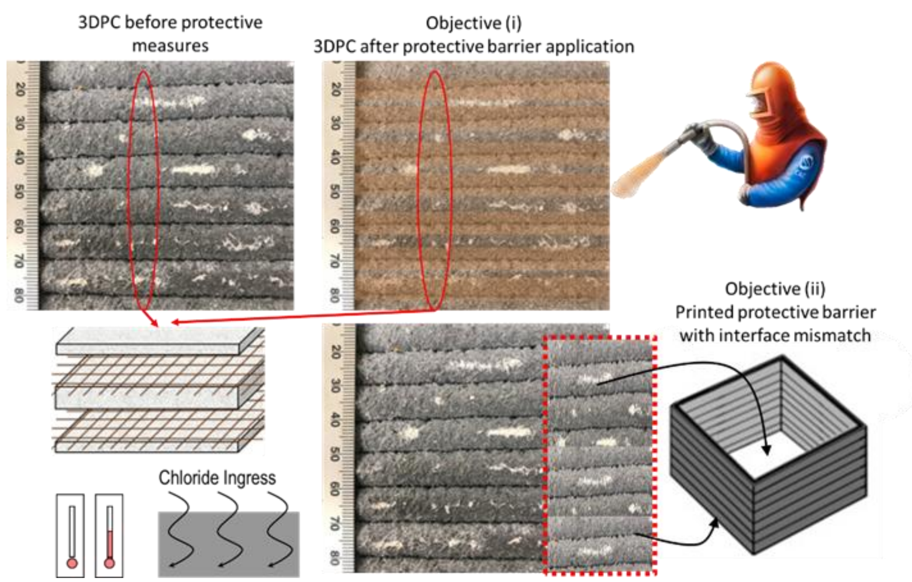

Figure 91: Schematic showing possible solutions

10.1.1 Protective Layer

Methods to protect the 3DPC interfaces by polymer surface finishings, by using a polymer resin on the interface, which creates an impenetrable barrier system against the aggressive ions, which can be seen in Figure 92. Also, the non-exposed and chemically exposed beams were tested after 90 days, which gives a very similar peak and post-peak behavior that implies the protective layer is doing its job perfectly which is displayed in Figure 93.

a) b)

Figure 92: (a)(b) Resin+hardener mix applied to the layers to prevent deterioration

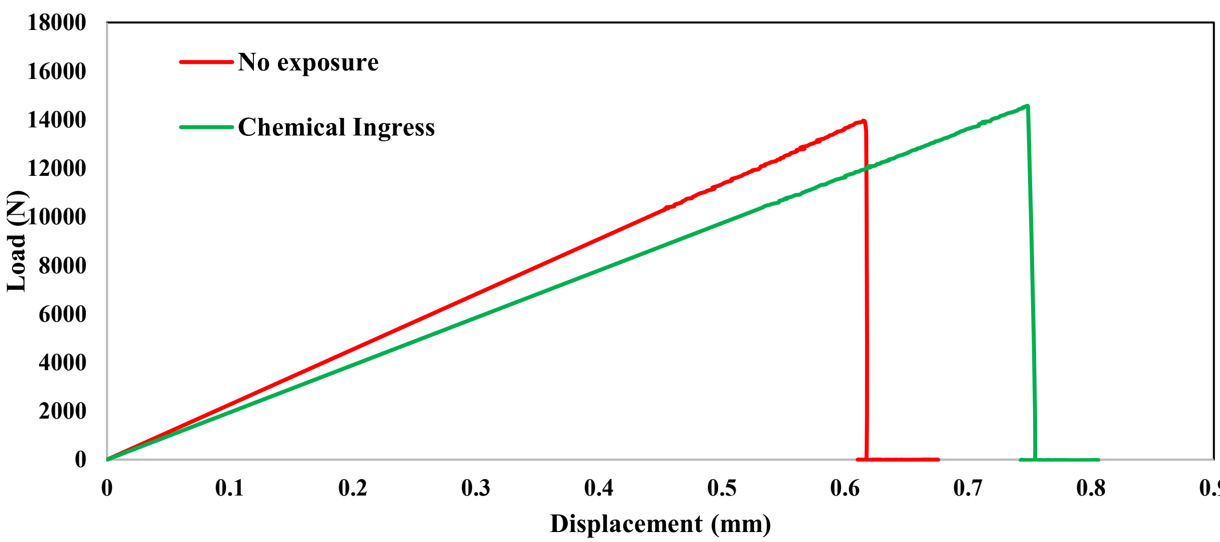

Figure 93: Load vs Displacement for protective layer solution beams after 90 days of testing

10.1.2 Interface Mismatch

Investigate and modify the design to create a strategic interface mismatch where the interface can allow ingress, but due to a mismatch of the outer protection system, ingress is significantly reduced. On the other hand, the same 3D printed mix will ensure homogeneity and bond with printed systems. This can be seen in Figure 94.

Figure 94: Interface mismatch to prevent deterioration

11 Technology Transfer and Community Engagement Activities

11.1 Lexington Public School Visit

I, alongside my team, hosted 25 middle school students from Lexington Public School in the Fears lab to educate them on the benefits and design flexibility of 3D printing technologies. The students were thrilled to experience concrete reinforcement materials and had an opportunity to visualize the strength of concrete through an ASTM standard test. They were also fascinated by the concrete 3D printer's movement, its robotic arm, as they were familiar with robotic science. Figure 95 shows the students with 3D printers and printed elements.

a)

b)

Figure 95: (a) Lexington School students observing concrete 3D Printer (b) Lexington School students observing 3D printed polymers

11.2 National Summer Transportation Institute (NSTI) Workshop

The team hosted 12 high school youths from different parts of the state in Fears' lab to get them trained on the basics of 3D printing and its perks. The workshop was backed up by the National Summer Transportation Institute (NSTI). Based on the students' feedback, the NSTI survey targeted their comprehension and attitudes towards 3D printing before and after the workshop and measured them through hands-on experience. The outcomes explicitly pointed to enhanced knowledge and excitement post the session, as the students were more than ever ready to share how electronic models come to be and the whole process of 3D printing with materials like concrete. The students' perception of 3D printing in construction being a game changer in the areas of time, money, and environmental impact grew tremendously. Students were also able to express the idea of reinforcement in printed concrete structures and could even cite real-world project applications for this technology in infrastructure like roads and bridges. The participants' level of interest and curiosity about 3D printing in construction was consistently high throughout the workshop, and almost everyone agreed that it was a very exciting development. Not only this, students' motivation towards STEM and civil engineering careers was positively influenced by the workshop, as many confessed, they could get involved with such technologies someday. All in all, the evidence shows that the workshop was a success in that it improved students' knowledge, self-esteem, and interest in future careers that are linked to 3D printing in construction. Figure 96 shows the NSTI workshop for 3D printing and learning.

a)

b)

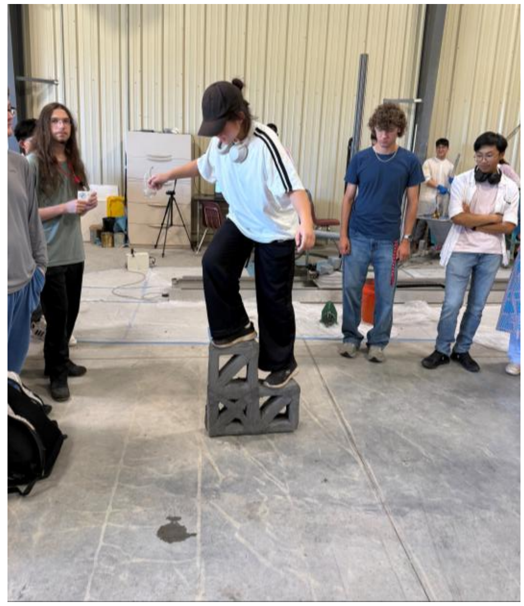

c)

Figure 96: (a)(b)(c) NSTI workshop for 3D printing and learning

References

1. Adhikari, S., et al., *Thermoplastic carbon fiber reinforced polymer tapes in cementitious and polymer concretes.* Functional Composites and Structures, 2025. **7**(2): p. 025005.
2. Adhikari, S., et al., *Scanning electron microscopy of carbon nanotube–epoxy interfaces: Correlating morphology to sulfate exposure.* Journal of Composites Science, 2025. **9**(8): p. 392.
3. USDOT FHWA; Available from: ://www.fhwa.dot.gov/bridge.
4. Shahrubudin, N., T.C. Lee, and R. Ramlan, *An overview on 3D printing technology: Technological, materials, and applications.* Procedia manufacturing, 2019. **35**: p. 1286-1296.
5. Gebler, M., A.J.S. Uiterkamp, and C. Visser, *A global sustainability perspective on 3D printing technologies.* Energy policy, 2014. **74**: p. 158-167.
6. Sanjayan, J.G., et al., *Effect of surface moisture on inter-layer strength of 3D printed concrete.* Construction and building materials, 2018. **172**: p. 468-475.
7. Marchment, T., J. Sanjayan, and M. Xia, *Method of enhancing interlayer bond strength in construction scale 3D printing with mortar by effective bond area amplification.* Materials & Design, 2019. **169**: p. 107684.
8. ABrAMS, D.A., *Design of concrete mixtures*. Vol. 1. 1919: Structural Materials Research Laboratory, Lewis Institute.
9. Roussel, N. and F. Cussigh, *Distinct-layer casting of SCC: The mechanical consequences of thixotropy.* Cement and Concrete Research, 2008. **38**(5): p. 624-632.
10. Tay, Y.W.D., et al., *Time gap effect on bond strength of 3D-printed concrete.* Virtual and Physical Prototyping, 2019. **14**(1): p. 104-113.
11. Austin, S., P. Robins, and Y. Pan, *Tensile bond testing of concrete repairs.* Materials and structures, 1995. **28**: p. 249-259.
12. Mohamed, O.A., M.A. Kewalramani, and A.M. Imran, *Shear and flexure of FRP-reinforced concrete beams and slabs–A review.* Materials Today: Proceedings, 2023.
13. Katz, A., *Environmental impact of steel and fiber–reinforced polymer reinforced pavements.* Journal of Composites for Construction, 2004. **8**(6): p. 481-488.
14. Feng, G., et al., *A review on mechanical properties and deterioration mechanisms of FRP bars under severe environmental and loading conditions.* Cement and Concrete Composites, 2022. **134**: p. 104758.
15. Erenstone, J., *3D Printed Prostheses: The Path from Hype to Reality.* Canadian Prosthetics & Orthotics Journal, 2023. **6**(2): p. 42141.
16. Tetsuka, H. and S.R. Shin, *Materials and technical innovations in 3D printing in biomedical applications.* Journal of Materials Chemistry B, 2020. **8**(15): p. 2930-2950.
17. Piazza, M. and S. Alexander, *Additive manufacturing: a summary of the literature.* 2015.
18. Su, A. and S.J. Al'Aref, *History of 3D printing*, in *3D printing applications in cardiovascular medicine*. 2018, Elsevier. p. 1-10.
19. Lipson, H., et al., *3-D printing the history of mechanisms.* 2005.
20. Jadhav, A. and V.S. Jadhav, *A review on 3D printing: An additive manufacturing technology.* Materials Today: Proceedings, 2022. **62**: p. 2094-2099.
21. Nerella, V.N., S. Hempel, and V. Mechtcherine, *Effects of layer-interface properties on*

mechanical performance of concrete elements produced by extrusion-based 3D-printing. Construction and Building Materials, 2019. **205**: p. 586-601.
22. De Schutter, G., et al., *Vision of 3D printing with concrete—Technical, economic and environmental potentials.* Cement and Concrete Research, 2018. **112**: p. 25-36.
23. Bos, F., et al., *Additive manufacturing of concrete in construction: potentials and challenges of 3D concrete printing.* Virtual and physical prototyping, 2016. **11**(3): p. 209-225.
24. Buswell, R.A., et al., *3D printing using concrete extrusion: A roadmap for research.* Cement and concrete research, 2018. **112**: p. 37-49.
25. Wangler, T., et al., *Digital concrete: opportunities and challenges.* Rilem technical letters, 2017. **1**(1): p. 67-75.
26. Zhang, C., et al., *Mix design concepts for 3D printable concrete: A review.* Cement and Concrete Composites, 2021. **122**: p. 104155.
27. Paul, S.C., et al., *A review of 3D concrete printing systems and materials properties: Current status and future research prospects.* Rapid Prototyping Journal, 2018. **24**(4): p. 784-798.
28. Perrot, A., D. Rangeard, and A. Pierre, *Structural built-up of cement-based materials used for 3D-printing extrusion techniques.* Materials and Structures, 2016. **49**: p. 1213-1220.
29. Ogura, H., V.N. Nerella, and V. Mechtcherine, *Developing and testing of strain-hardening cement-based composites (SHCC) in the context of 3D-printing.* Materials, 2018. **11**(8): p. 1375.
30. Bos, F.P., et al., *Experimental exploration of metal cable as reinforcement in 3D printed concrete.* Materials, 2017. **10**(11): p. 1314.
31. Mechtcherine, V. and V.N. Nerella, *Integration der Bewehrung beim 3D-Druck mit Beton.* Beton-und Stahlbetonbau, 2018. **113**(7): p. 496-504.
32. El Inaty, F., B. Baz, and G. Aouad, *Long-term durability assessment of 3D printed concrete.* Journal of Adhesion Science and Technology, 2023. **37**(12): p. 1921-1936.
33. Miryousefi Ata, S., A. Kazemian, and A. Jafari. *Application of concrete 3D printing for bridge construction: Current challenges and future directions*. in *Construction Research Congress 2022*. 2022.
34. Le, T.T., et al., *Hardened properties of high-performance printing concrete.* Cement and concrete research, 2012. **42**(3): p. 558-566.
35. Nishiwaki, T., et al., *Reinforcing interlayers of three-dimensional-printed mortar using metal fiber insertion.* ACI Materials Journal, 2021. **118**(6): p. 331-340.
36. Zhang, Y., et al., *Interlayer adhesion of 3D printed concrete: Influence of layer stacked vertically.* Construction and Building Materials, 2023. **399**: p. 132424.
37. Haibe, A.A., *Investigation of flexural behavior of reinforced concrete with 3D printed glass fiber reinforced polymer.* 2022.
38. Ambily, P.S., N. Rajendran, and S.K. Kaliyavaradhan, *Mix design, optimisation and performance evaluation of three-dimensional printable concrete.* Proceedings of the Institution of Civil Engineers-Construction Materials, 2023: p. 1-19.
39. Murcia, D.H., et al., *Flexural behavior of a novel textile-reinforced polymer concrete.* Polymers, 2022. **14**(1): p. 176.
40. Guo, J., et al., *Damage mechanism and modeling of concrete in freeze–thaw cycles: a review.* Buildings, 2022. **12**(9): p. 1317.

41. Fagerlund, G., *The critical degree of saturation method of assessing the freeze/thaw resistance of concrete.* Matériaux et Construction, 1977. **10**: p. 217-229.
42. Wang, L., et al., *Freeze-thaw resistance of 3D-printed composites with desert sand.* Cement and Concrete Composites, 2022. **133**: p. 104693.
43. Warsi, S.B.F., B. Panda, and P. Biswas, *Exploring fibre addition methods and mechanical properties of fibre-reinforced 3D printed concrete: A review.* Developments in the Built Environment, 2023: p. 100295.
44. ASTM International, *C666 Standard Test Method for Resistance of Concrete to Rapid Freezing and Thawing*. 2024: West Conshohocken, PA, USA.
45. Zhang, Y., et al., *Hardened properties and durability of large-scale 3D printed cement-based materials.* Materials and Structures, 2021. **54**: p. 1-14.
46. Siddika, A., et al., *3D-printed concrete: Applications, performance, and challenges.* Journal of Sustainable Cement-Based Materials, 2020. **9**(3): p. 127-164.
47. Van Der Putten, J., et al. *3D printing of concrete: the influence on chloride penetration*. in *RILEM International Conference on Concrete and Digital Fabrication*. 2020. Springer.
48. Malan, J.D.M., A.S. van Rooyen, and G.P. van Zijl, *Chloride induced corrosion and carbonation in 3D printed concrete.* Infrastructures, 2021. **7**(1): p. 1.
49. Baz, B., et al., *Durability assessment and microstructural analysis of 3D printed concrete exposed to sulfuric acid environments.* Construction and Building Materials, 2021. **290**: p. 123220.
50. ASTM International, *C1437 Standard Test Method for Flow of Hydraulic Cement Mortar*. 2020: West Conshohocken, PA, USA.
51. ASTM International, *C191-18a Standard Test Methods for Time of Setting of Hydraulic Cement by Vicat Needle*. 2019: West Conshohocken, PA, USA.
52. ASTM International, *C109 Standard Test Method for Compressive Strength of Hydraulic Cement Mortars (Using 50 mm [2 in.] Cube Specimens)*. 2024: West Conshohocken, PA, USA.
53. Cardenas, H., K. Kupwade-Patil, and S. Eklund, *Recovery from sulfate attack in concrete via electrokinetic nanoparticle treatment.* Journal of materials in civil engineering, 2011. **23**(7): p. 1103-1112.
54. Heras Murcia, D., *3D PRINTED CONCRETE & POLYMER CONCRETE FOR INFRASTRUCTURE APPLICATIONS.* 2021.
55. Murcia, D.H., *3D Printed Concrete & Polymer Concrete for Infrastructure Applications*. 2021: The University of New Mexico.